Technical

NASA CR-145142

F-C4188-1

Report

WIND TUNNEL TESTS OF THE DYNAMIC CHARACTERISTICS OF THE FLUIDIC RUDDER

By

Charles A. Belsterling

Prepared under Contract No. NAS1-13930

By

The Franklin Institute Research Laboratories
Philadelphia, Pennsylvania 19103

December, 1976

for

NASA
National Aeronautics and
Space Administration

THE FRANKLIN INSTITUTE RESEARCH LABORATORIES
THE BENJAMIN FRANKLIN PARKWAY · PHILADELPHIA, PENNSYLVANIA 19103

1. Report No.	2. Government Accession No.	3. Recipient's Catalog No.
ASA CR-145142		

4. Title and Subtitle	5. Report Date
Wind Tunnel Tests of the Dynamic Characteristics of the Fluidic Rudder	December 1976
	6. Performing Organization Code
7. Author(s)	8. Performing Organization Report No.
Charles A. Belsterling	F-C4188-1
	10. Work Unit No.
9. Performing Organization Name and Address	
The Franklin Institute Research Laboratories Philadelphia, Pennsylvania 19103	11. Contract or Grant No. NAS1-13930
	13. Type of Report and Period Covered
12. Sponsoring Agency Name and Address	Contractor Report 6/75-12/76
Langley Research Center National Aeronautics and Space Administration Hampton, Virginia 23665	14. Sponsoring Agency Code

15. Supplementary Notes

Final Report. NASA Project Manager, H. Douglas Garner
Flight Instrument Division

16. Abstract

This report covers the fourth phase of a continuing program to develop the means to stabilize and control aircraft without moving parts or a separate source of power. Previous phases have demonstrated the feasibility of 1) generating adequate control forces on a standard airfoil, 2) controlling those forces with a fluidic amplifier and 3) cascading non-vented fluidic amplifiers operating on ram air supply pressure. The foremost objectives of the fourth phase covered under Part I of this report were to demonstrate a complete force-control system in a wind tunnel environment and to measure its static and dynamic control characteristics. Secondary objectives, covered under Part II, were to evaluate alternate configurations for lift control. The results demonstrate an overall response time of 150 msec, confirming this technology as a viable means for implementing low-cost reliable flight control systems.

17. Key Words (Suggested by Author(s))	18. Distribution Statement
Flight control Aircraft stabilization Fluidics Aerodynamics	Unclassified - Unlimited

19. Security Classif. (of this report)	20. Security Classif. (of this page)	21. No. of Pages	22. Price*
Unclassified	Unclassified	40	

* For sale by the National Technical Information Service, Springfield, Virginia 22151

NASA CR-145142

WIND TUNNEL TESTS OF THE DYNAMIC CHARACTERISTICS OF THE FLUIDIC RUDDER

By

Charles A. Belsterling

Prepared under Contract No. NAS1-13930

By

The Franklin Institute Research Laboratories
Philadelphia, Pennsylvania 19103

December, 1976

for

National Aeronautics and
Space Administration

CONTENTS

FIGURES

FIGURES (CONTINUED)

WIND TUNNEL TESTS OF THE DYNAMIC CHARACTERISTICS OF THE FLUIDIC RUDDER

By Charles A. Belsterling
Franklin Institute Research Laboratories

INTRODUCTION

This report covers the fourth phase of a continuing program to develop the means to stabilize and control aircraft without moving parts or a separate source of power. Previous phases (refs. 1 and 2) have demonstrated the feasibility of 1) generating adequate control forces on a standard airfoil, 2) controlling those forces with a fluidic amplifier and 3) cascading non-vented fluidic amplifiers operating on ram air supply pressure. The foremost objectives of the fourth phase covered under Part I of this report were to demonstrate a complete force-control system in a wind tunnel environment and to measure its static and dynamic control characteristics. The approach was to build a wind tunnel model airfoil including a scoop and cascaded fluidic amplifiers, instrument the amplifiers with electronic pressure transducers and the model with lift and drag transducers, and provide the means for introducing incremental and step changes in signals to the first stage fluidic control amplifier. Secondary objectives, covered under Part II, were to evaluate alternate configurations for lift control. This was done by modifying a laboratory test facility into the form of a miniature wind tunnel and measuring the lift of three model airfoils with six different slot configurations.

PART I - DYNAMIC TESTS OF THE FLUIDIC RUDDER

Wind Tunnel Model

The basic structure of the wind tunnel model is an 85 cm (33.5 in.) section of the tip of the vertical tail of a Cessna 177 aircraft. The airfoil is a symmetrical NACA 0008 section and it is tapered and swept back as shown in the planform view in Figure 1.

The model airfoil is fitted with a round ram air scoop at its root with a frontal area of 154 sq. cm (23.9 sq. inches). Details of the scoop design are shown in Figure 2. It is designed to collect ram air and deliver it to the sealed plenum chamber inside the airfoil with a pressure recovery of better than 75% (75% of the dynamic pressure).

The recovered pressure is controlled by internal fluidic amplifiers to direct flow from spanwise slots in the aerodynamic section at approximately 55% chord, just forward of the existing hinged rudder. There are three sets of slots in the airfoil surfaces, each slot approximately

1.52 cm (0.60 in.) by 25.4 cm (10.0 in.) for a total area in one surface of 116 sq. cm (18 sq. in.) to which the scoop frontal area is roughly matched. The model airfoil as delivered to the wind tunnel is shown in Figure 3.

Fluidic Amplifiers

Inside the model airfoil are three sets of cascaded fluidic amplifiers typically arranged as shown in Figure 4. The ram air pressure recovered in the plenum chamber is the power supply for the cascaded pair of amplifiers in each set. Because the pressure just outside the slots is normally lower than the plenum pressure there is always flow through the fluidic amplifier power nozzles which form the flow into a jet sheet that can be deflected with differential control signals. Under balanced conditions ($\Delta P1 = 0$) the driver amplifier power jet is undeflected so the flow is evenly divided into the control chambers of the slot flow amplifier ($\Delta P2 = 0$). Then the slot flow amplifier is also undeflected so the flow velocity out the slots in both aerodynamic surfaces is equal (differential total pressure, $\Delta P3 = 0$) and the effect on the lift of the symmetrical airfoil is identical ($\Delta L = 0$).

When a control differential pressure is applied to the driver amplifier ($\Delta P1$ of a positive sense), the power jet is deflected toward the opposite output leg so the differential pressure recovered in the control chambers of the slot flow amplifiers is not zero ($\Delta P2$ of a negative sense). This deflects the power jet of the slot flow amplifier to direct more flow from the slots in one aerodynamic surface than from the slots in the other side ($\Delta P3$ of a positive sense). The excess results in a decrease in effective lift on that surface and an increase in effective lift on the other side and there is a net force perpendicular to the plane of the airfoil (ΔL in the same sense as $\Delta P1$). Since each stage of fluidic amplification provides flow gain, this arrangement makes possible the control of large aerodynamic forces by means of a low-power air signal.

The amplifiers in the wind tunnel model are designed according to the optimum dimensions established in the preceeding phase of the program (ref. 2). A dimensional drawing of a typical slot flow amplifier is shown in Figure 5. Because of the airfoil taper, the envelope dimensions of each of the three in the airfoil are different but the critical dimensions relative to the power nozzle are identical.

When construction of the wind tunnel model was started, it was found that the envelope dimensions of the driver amplifier defined in the previous phase of the program (ref. 2) were too large to fit inside with the necessary interconnecting ductwork. The design was modified as shown in Figure 6 including miniature air cylinders for delay-free remote control of the input signals. The cylinders are actuated with 17.2 N/cm^2 (25 psi) air from outside the wind tunnel to alternately close and open the rectangular ports leading from the plenum chamber inside the airfoil to

the control chambers of the driver amplifier.

The output of each driver amplifier is connected to its respective slot flow amplifier through rectangular ducts. They fan out from the 5.1 cm (2 in.) wide output ports of the driver to mate with the 22.9 cm (9 in.) inlet (control) ports of the slot flow amplifier. Figure 7 shows one complete assembly of amplifiers as they are arranged inside the airfoil where the output ports of the slot flow amplifier are aligned with the slots in the skin.

Instrumentation

The Phase 4 wind tunnel model is provided with the instrumentation to measure static and dynamic characteristics of the fluidic amplifiers and the airfoil. Pressure taps are located to detect the following quantities statically:

- recovered pressure in plenum (2)
- airfoil skin pressure @ 20% chord both sides
- control pressures to the driver amplifier (2)
- output flow as indicated by the difference in total pressure from probes pointed upstream in slots

They were read out on an alcohol-filled manometer board with tunnel total and static pressures. The other static quantities of interest, lift, drag and pitch angle, were read from the wind tunnel balance console.

For dynamic tests the wind tunnel model is fitted with electronic transducers to detect the following:

- differential control pressure to the driver amplifier ($\Delta P1$)
- differential control pressure to the slot flow amplifier ($\Delta P2$)
- differential output flow from the slots as measured with total pressure probes pointed upstream in the slots ($\Delta P3$)
- lift force
- drag force

The differential pressures are measured by miniature pressure transducers located inside the airfoil. Lift and drag are measured with special model mounting attachments fitted with strain gages and located at the three points where the model is supported by the wind tunnel balance struts. Typical units are shown in Figure 8. These units are designed to measure lift in tension and drag in bending. The two quantities can be sampled by means of the electronic signal conditioning equipment outside the tunnel.

The dynamic variables are recorded simultaneously on a 4-channel strip-chart recorder. A typical readout is shown in Figure 9. The top

trace (Channel 1) is the differential control signal to the driver amplifier, $\Delta P1$. Channel 2 is the differential control pressure to the slot flot amplifier, $\Delta P2$. Channel 3 is the differential output flow from the slots in the airfoil, $\Delta P3$. Channel 4 can be either lift, L, or drag, D, sampled alternately.

Note that all dynamic readouts can be calibrated against static readouts after installation of the model in the wind tunnel.

Wind Tunnel Tests

The major objective of the series of wind tunnel tests conducted under Phase 4 of the program was to record the dynamic characteristics of the fluidic rudder under simulated in-flight conditions. A prerequisite to meeting this objective was to measure static characteristics to insure that the new scoop and the fluidic amplifiers were performing as designed. This was also necessary to calibrate the dynamic instrumentation and to confirm correlation with previous wind tunnel tests.

A secondary objective was to further investigate the coupling between slot flow control of aerodynamic forces and conventional rudder control. Previous wind tunnel test results (ref. 1) showed that the induced rudder hinge moments were in the direction to aid slot flow control. In either of these tests the investigation was to cover the case of a free rudder, to establish if there was any tendency toward instability due to the dynamic coupling of the two types of control.

To provide the data to meet the objectives of this phase of the program, three studies were conducted as follows:

1. static tests with fixed rudder at angles of attack of the airfoil, -2°, 0°, +2°, +14° varying the command signal to the driver amplifier in increments
2. dynamic tests with fixed rudder at angles of attack of the airfoil, -2°, 0°, +2°, +4° applying "step" input control signals to the driver amplifier.
3. dynamic tests with free rudder at angles of attack of the airfoil, -2°, 0°, +2° applying "step" input control signals to the driver amplifier.

Figure 10 shows the Phase 4 model fluidic rudder mounted in the wind tunnel.

Test Results

The dynamic pressure ($P_T - P_S$) in the wind tunnel during nominal operation was approximately 18.7 cm of alcohol. The pressure recovered

inside the airfoil referred to tunnel static was 14.5 cm of alcohol. Therefore the recovery is better than 77% to be compared with 80% predicted from data taken in previous wind tunnel tests (ref. 1) for a frontal area of 154 cm^2.

Figure 11 shows the static lift control characteristics of the complete model fluidic rudder at zero angle. As in previous similar tests, the lift is proportional to the control signal, but the data points are scattered because of extreme aerodynamic noise. However, in these tests there is evidence of saturation, as expected, due to the characteristics of the fluidic amplifiers, but the saturating is limiting the maximum lift force.

Figure 12 relates lift changes to the flow from the airfoil slots. Again the control is proportional and, as predicted from previous tunnel tests, very nearly linear with differential total pressure.

Figure 13 shows the characteristics of the slot flow amplifier. Note that the amplifier is operating in a nearly linear range (not saturating) and the maximum pressure differential recovered in the slots is 66% of the recovered pressure in the plenum. This is of a magnitude expected from laboratory tests (ref. 2) but the non-saturating characteristic indicates that the driver amplifier is not providing enough control signal to produce maximum effect in both directions. There is some evidence of unbalance.

Figure 14 is a plot of the static characteristics of the cascaded pair. Since the slot flow amplifier is nearly linear (Figure 13) these curves indicate that the driver amplifier is saturating and limiting the output from the slot flow amplifier. Apparently the critical dimensions of the driver amplifier have been shifted from the optimum set used in previous laboratory tests. This may be a result of high temperatures in the wind tunnel during prolonged testing, 53.3°C (128°F).

Figure 15 is the measured characteristic of the driver amplifier. This confirms that it is slightly unbalanced and is saturating before driving the slot flow amplifier to maximum output.

Figure 16 shows the drag characteristics of the model fluidic rudder with balanced slot flows and at the two extremes of slot flows. Note that drag varies with angle of attack in the normal way (minimum at zero) but there is no significant change due to changes in the proportioning of slot flows. This is expected because the total through-flow is a constant for all conditions of control. Note that this is not the case for control with a moving surface.

Figures 17 and 18 are typical recordings of the dynamic response of the model fluidic rudder. Figure 17 shows the response of the fluidic amplifiers and lift of the airfoil. Channel 1 is the command signal to the driver amplifier ($\Delta P1$). Channel 2 ($\Delta P2$) shows that the driver

amplifier responds in approximately 10 msec as indicated by a comparison of the midpoints of the pressure change. Channel 3 ($\Delta P3$) shows that the slot flow amplifier responds, in turn, in approximately 15 msec or approximately 25 msec after the command signal. Note that considering the recovered pressure in the plenum and the distance the signal must travel, the recorded delay is in the order of the transport time of the air through the amplifiers. This indicates that the time constant due to compressibility is negligible, which is expected because the amplifiers are primarily flow diverters, not pressure amplifiers.

Channel 4 (ΔL) indicates the presence of a high level of aero-dynamic "noise" inducing oscillations in the lift measurements. The sensitivity of Channel 4 is set for a deflection of one cm for the step change. The unsteadiness in lift is as much as 5 to 10 times greater. However, by recording and studying a large number of responses, the total response time (90% of final value) of the fluidic rudder has been established as approximately 150 msec. The average response characteristic is sketched over the recording in Figure 17. Note that the response includes a second order lag due to model mass and mount deflection.

Figure 18 shows the dynamic response of the fluidic amplifiers and drag of the airfoil. In this test there was again a serious problem because of the effect of aerodynamic "noise" in the drag measurement. In this case the study of a large number of repeated recordings failed to uncover a significant response characteristic. The absence of a drag response was predicted by the static test data presented in Figure 16 that show, at a fixed angle of attack, there is no significant change in drag with changes in slot flow.

Table I summarizes the results of tests of the dynamic coupling between slot flows and the free rudder. With maximum flow from one set of slots the unrestrained rudder was left to seek its own angle of equilibrium, θ. Then the flow was suddenly switched to the opposite set of slots. The free rudder now seeks a new angle of equilibrium as follows:

TABLE I - FREE RUDDER ANGLE, θ

	ANGLE OF ATTACK, α		
	-2°	0°	+2°
Max. flow from top slots	-4°	-2 3/4°	-1 1/2°
Max. flow from bottom slots	-4 3/4°	-3 1/2°	-2 1/4°

As indicated, the rudder is not perfectly weight-balanced in the horizontal position so it assumes an average deflection in the downward direction. Then as the slot flows are instantaneously switched from the top to the bottom and return, the free rudder angle changes 3/4 degrees for angles of attack from -2° to +2°. The change is in the direction of

aiding slot flow control. That is, the rudder deflects toward the side with slot flow creating a net force in the opposite direction; the same direction as the force created by the slot flow.

Although the rudder was not instrumented for recording, the transient response was observed directly through the wind tunnel viewing window. There was no evidence of dynamic instability or low damping in the rudder response. In fact, the response appeared to be heavily over-damped.

Conclusions

The results of the wind tunnel tests of the model fluidic rudder lead to the following conclusions:

1. the new scoop design is a good match for the size of slots employed
2. the proportionality between slot flow and lift is once again confirmed
3. the slot flow amplifier is effective in controlling flow from the slots in the aerodynamic surfaces
4. cascaded fluidic amplifiers will operate inside the sealed airfoil under simulated in-flight conditions
5. the instrumented driver amplifier is saturating at a level below which maximum effect can be realized, probably because of dimensional shifts due to high temperatures in the wind tunnel
6. there is no significant change in drag of the scoop and slot equipped airfoil with slot flow because the total thru-flow is constant
7. the response time of the driver amplifier is approximately 10 msec at a velocity equivalent to q = 14.7 cm of water (5.8 in. of water)
8. the response time (90% of final value) of the cascaded pair of fluidic amplifiers is approximately 25 msec at a velocity equivalent to q = 14.7 cm of water
9. the overall response time of lift on the model fluidic rudder is approximately 150 msec at a velocity equivalent to q = 14.7 cm of water, including a second order lag due to model mass and mount deflection
10. there is no significant dynamic response of drag to slot flow control transients
11. there is no tendency toward dynamic instability in the coupling between a free rudder and slot flow control of lift and the coupling is in a positive sense

Summary

In summary the results of the wind tunnel tests of the model fluidic rudder satisfy every objective of Phase 4 of the development program. The data show once again that the concepts of a fluidic rudder and the control of aircraft without moving parts or a separate source of power are viable.

PART II - COMPARISON OF ALTERNATE SLOT CONFIGURATIONS

Scale Models

Three different scaled airfoil sections were constructed to be used in a direct comparison of alternate methods of direct lift control applicable to the fluidic rudder. All three are basically NACA 0018 sections with a 20.3 cm (8.0 in.) chord and a 19.1 cm (7.5 in.) span fitted with a 3.60 cm (1.42 in.) inside diameter scoop at midspan. Six different slot configurations were provided and identified as follows:

Model	Slots	Description
45 FWD	LE	Slots at 2.5% chord pointed forward 45° from the chord line
45 FWD	55	Slots at 55% chord pointed forward 45° from the chord line (same as in large-scale fluidic rudder)
45 AFT	LE	Slots at 2.5% chord pointed aft 45° from the chord line
45 AFT	55	Slots at 55% chord pointed aft 45° from the chord line
RTE	AFT	Slots at rounded trailing edge pointed aft for Coanda attachment
RTE	45 FWD	Slots at rounded trailing edge pointed forward approximately 45° from chord line (see Figure 21)

The three models are shown in cross-section in Figures 19, 20 and 21. They are also shown as tested in Figure 22. Note that they are constructed in three span-wise sections with the scoop occupying most of the leading edge of the center section. Since leading edge slots could not be located there, only the outboard sections were fitted with 0.72 cm (0.28 in.) slots in all cases except Model RTE where 0.48 cm (0.19 in.) slots spanned all three sections. In this way the direct comparison of the effect of slots is valid because the active slot area and the ratio of scoop area to slot area is the same in all cases. Note that the ratio of slot area to total airfoil area is 0.0236, nearly 70% greater than the ratio in the wind tunnel model in Part I.

Test Facility

The three models described above were tested for static lift characteristics in the miniature wind tunnel facility shown in Figure 23. It is powered by a squirrel-cage blower capable of creating a wind velocity of more than 50 knots in the rectangular test section 20.3 cm (8.0 in.) by 12.7 cm (5.0 in.). The models are mounted on three vertical rods that extend through the floor of the test section to attach to three brackets fitted with strain gages as shown in Figure 24. The strain gages on all three brackets are connected in series so the resulting electrical output is proportional to the sum of the lift detected by all three; the total lift on the airfoil. The electrical output signal is measured with a four-place digital voltmeter, and the dynamic pressure at the entrance to the test section is monitored with an airspeed indicator.

Test Methods

To maintain the validity of the direct comparisons and to minimize the effect of reading errors, tests were conducted in the following sequence:

1. Each airfoil was covered with pressure-sensitive tape to close all slots.
2. The airfoil was mounted in the test section and adjusted for angle of attack.
3. A lift reading and a drag reading were taken before starting the blower.
4. After the blower was started the air flow was allowed to stabilize for one minute than a second lift and an airspeed reading were taken.
5. At zero angle of attack (only), a second drag reading was recorded.
6. One minute after the blower had been completely stopped a third lift reading and drag reading were taken.
7. The actual lift and actual drag were calculated as the difference between the second reading and the average of the first and third readings.
8. The sequence was repeated for angles of -2°, 0°, +2°, +4° and +6°.
9. After the "clean" airfoil had been tested a set of surface slots was opened with a razor blade and the sequence 1 through 8 repeated.

10. After one set of slots had been tested, they were closed with tape and the second set opened with a razor blade.

11. At the conclusion of the series of tests the lift measuring system was calibrated with dead weights and the drag measuring system was calibrated with a string scale.

Test Results

Figure 25 shows the results of tests on the model airfoil with forward-pointing slots (45 FWD). The clean airfoil with open scoop develops a normal lift characteristic symmetrical around zero angle of attack. The open leading edge slots produce a lift increment of 2.0 newtons (0.45 lbs.) at zero angle of attack. The slots at 55% chord produce a lift increment of 7.5 newtons (1.69 lbs.).

Figure 26 shows the results of tests on the model airfoil with aft-pointing slots (45 AFT). The clean airfoil develops a normal lift characteristic similar to the previous model. The open leading edge slots produce a lift increment of only 1.5 newtons (0.33 lbs.). The slots at 55% chord produce a lift increment of 3.0 newtons (0.67 lbs.).

Figure 27 shows the results of tests on the model airfoil with rounded trailing edge (RTE). The clean airfoil develops a lift characteristic somewhat steeper than normal. The slots pointed aft over the rounded trailing edge produce a lift increment of only 2.0 newtons (0.45 lbs.). However, the slots pointed forward at 45° produce a lift increment of 8.5 newtons (1.91 lbs.), only 13% more than the slots located at 55% chord.

Figure 28 shows the comparison between the most effective models in terms of lift versus drag. The results indicate that there is no significant difference.

Conclusions

Within the constraints of the experiments with alternate slot configurations, the following conclusions were reached:

1. Slots directed forward 45° with respect to the chord line are most effective.

2. Slots located at 55% chord or aft to the trailing edge are most effective.

3. Slots located at 55% chord result in lift/drag characteristics as efficient as slots at the trailing edge

4. At the low ejection velocities achievable with ram air, the Coanda effect cannot be depended upon to guide trailing edge jets perpendicular to the chord line.

5. The magnitude of the control forces developed by this method can be increased by opening larger slots and matching scoop area to slot area.

Summary

In summary the comparison of alternate slot configurations confirms, once again, that the concept of scoop-fed slots is a valid means for implementing no-moving-parts aerodynamic controls for many applications.

Franklin Institute Research Laboratories
20th & The Parkway
Philadelphia, Pennsylvania 19103
December 10, 1976

References

1. "Wind Tunnel Tests of a Symmetrical Airfoil with Scoop-Fed Slots", C. A. Belsterling, NASA CR-132568, November 1974.

2. "Development of an Advanced Fluidic Rudder System", C. A. Belsterling, NASA CR-144985, May 1976.

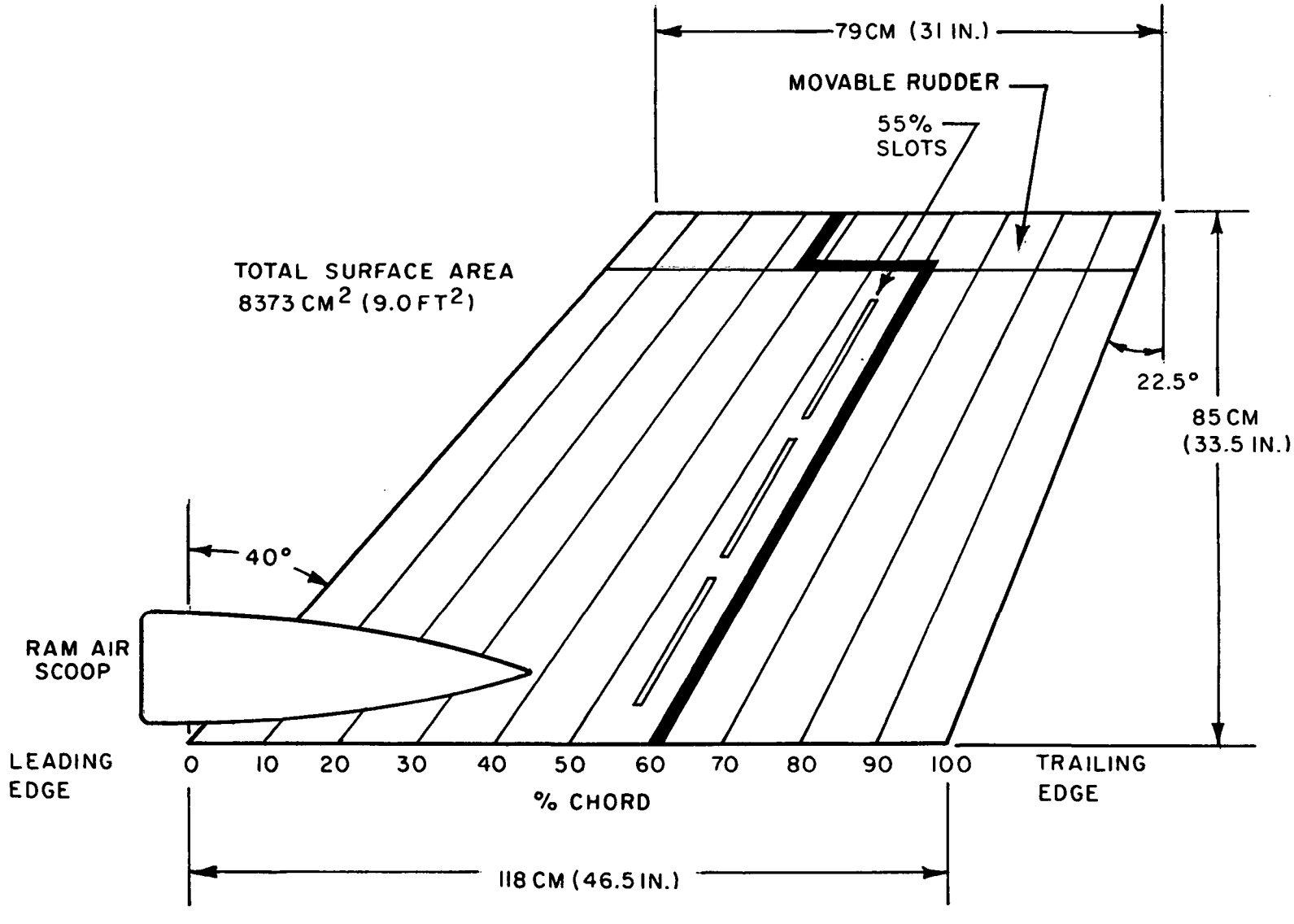

Figure 1. Plan View of Wind Tunnel Model Fluidic Rudder

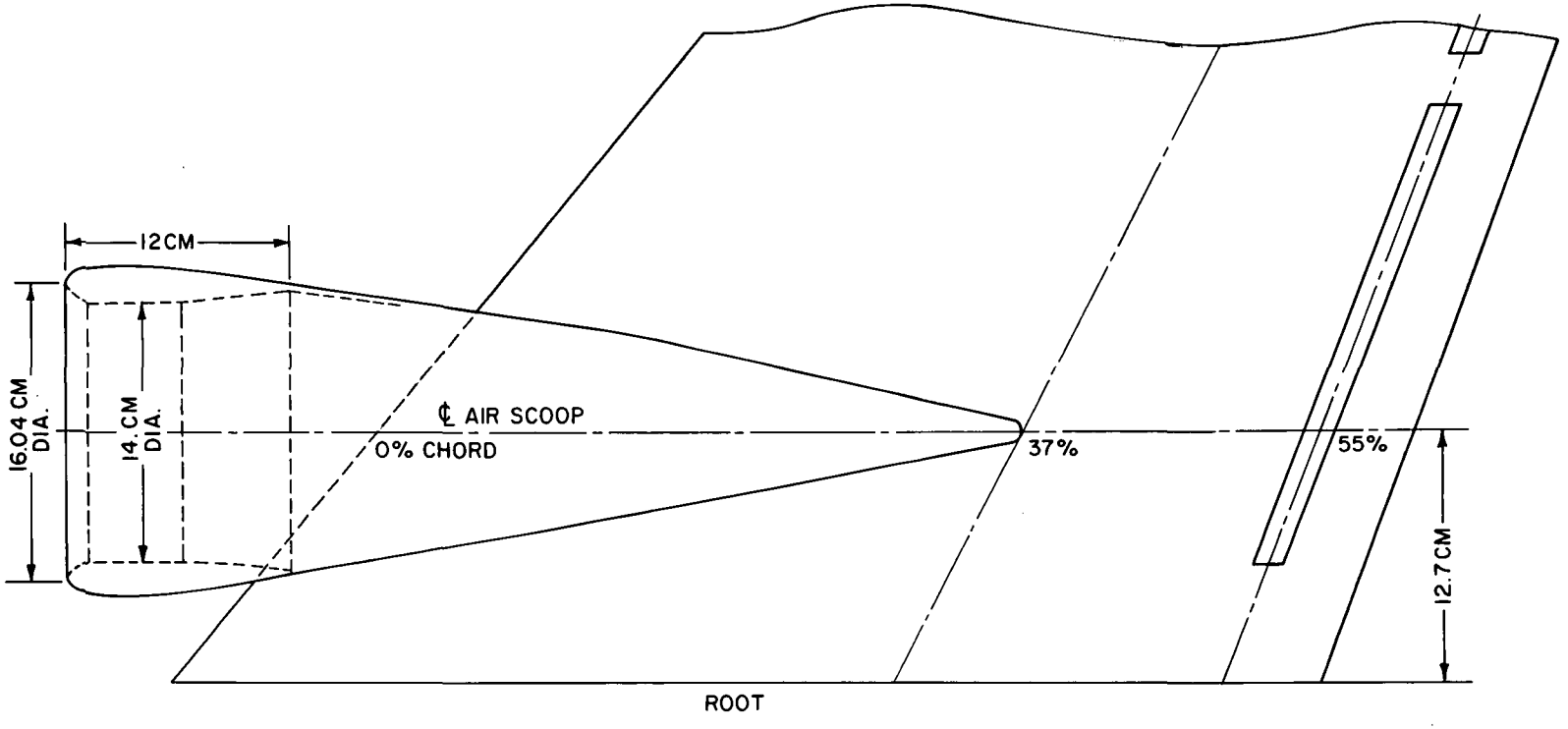

Figure 2. Details of Ram Air Scoop

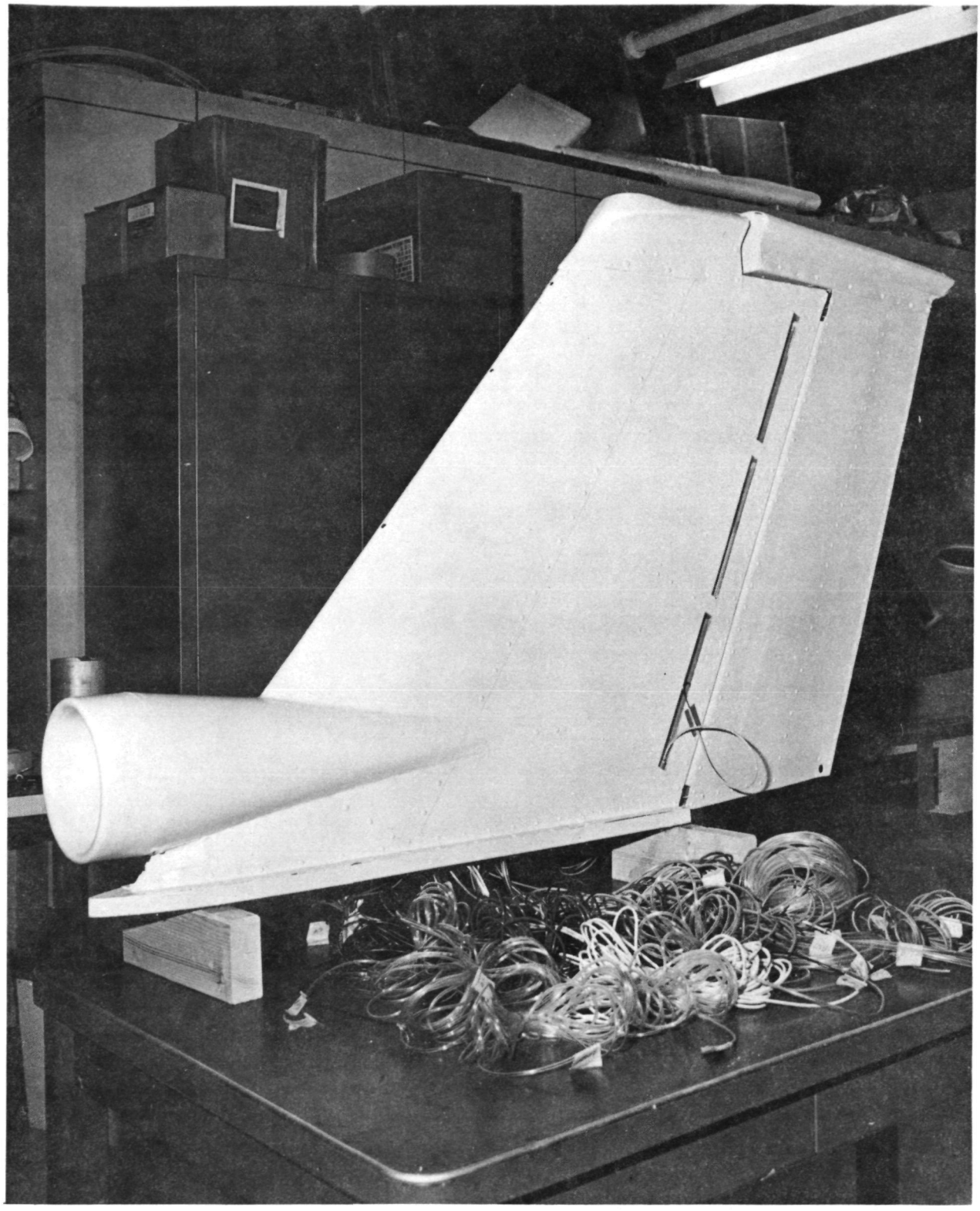

Figure 3. Photo of Model Rudder as Delivered to the Wind Tunnel

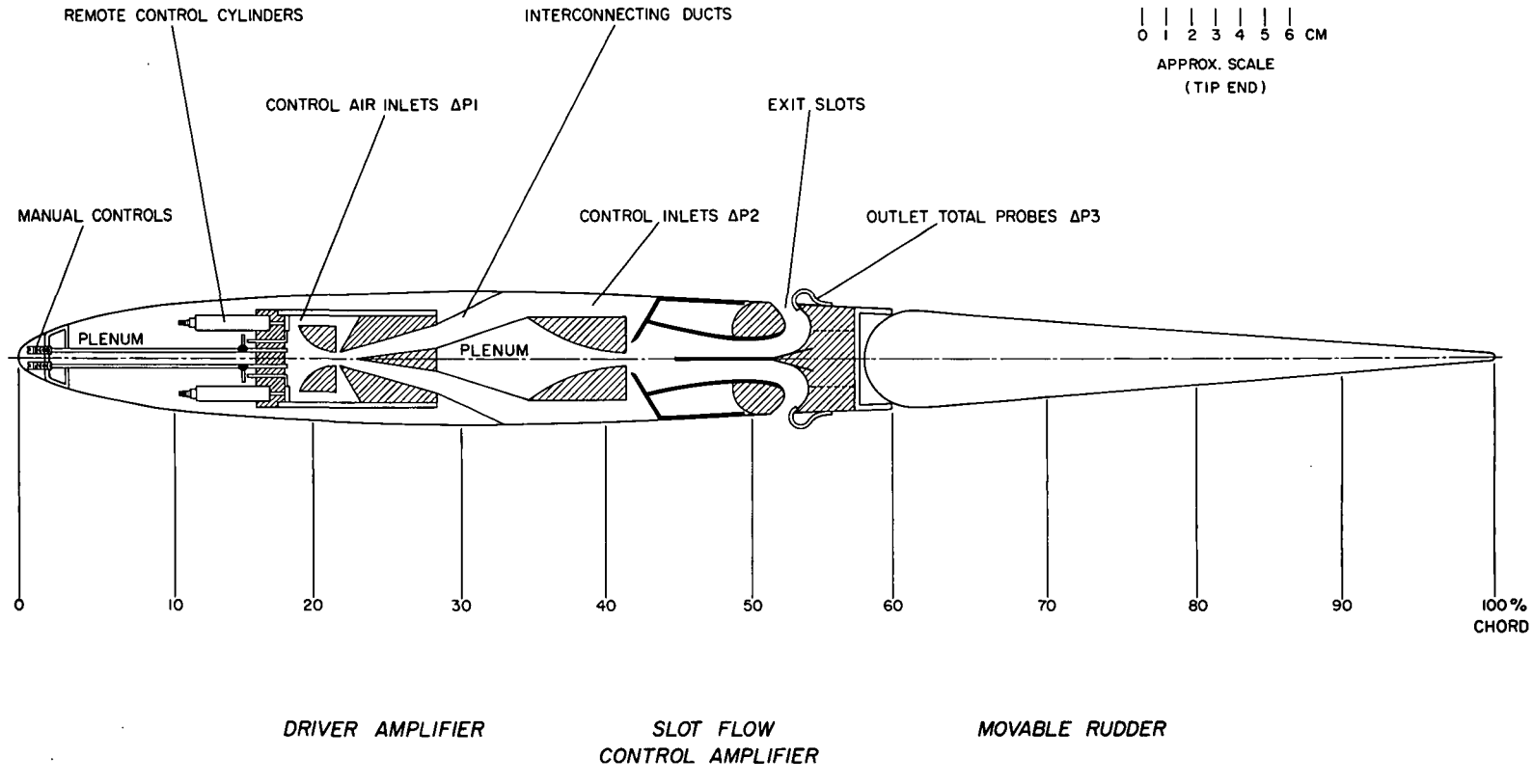

Figure 4. Cross Section of Model Rudder Showing Arrangement of Fluidic Amplifiers

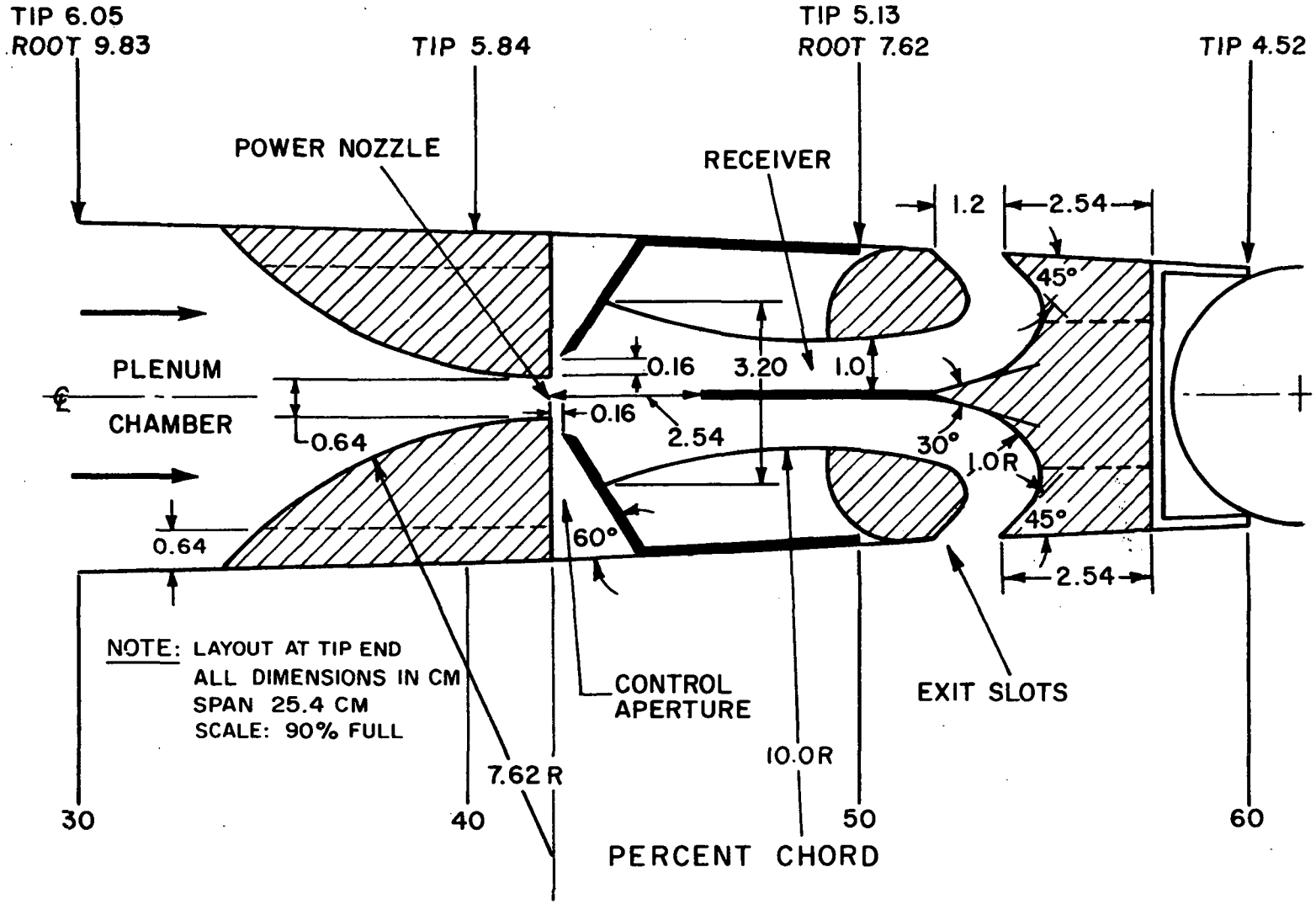

Figure 5. Dimensions of Typical Slot Flow Amplifier

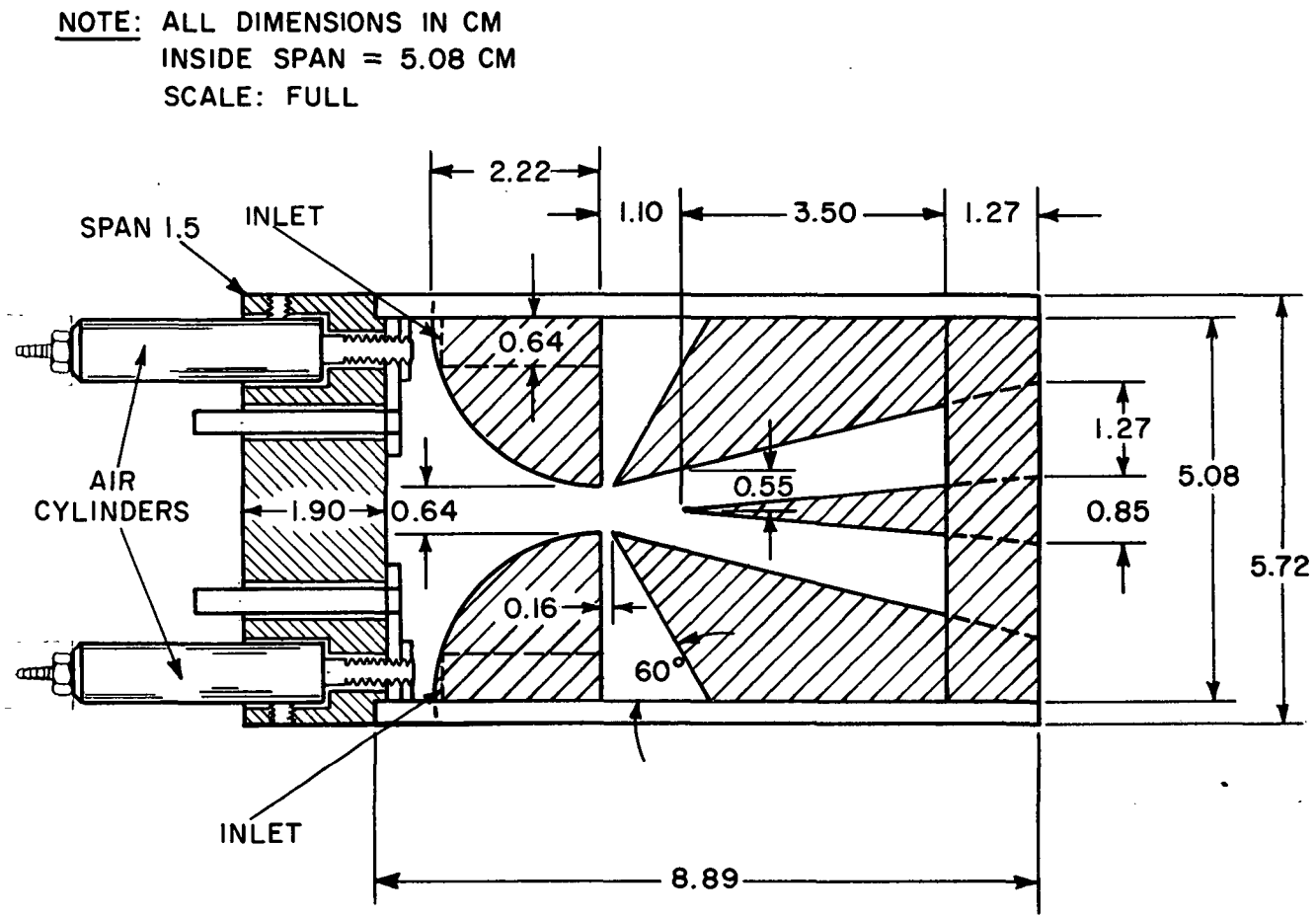

Figure 6. Miniaturized Driver Amplifier With Remote Control Inlets

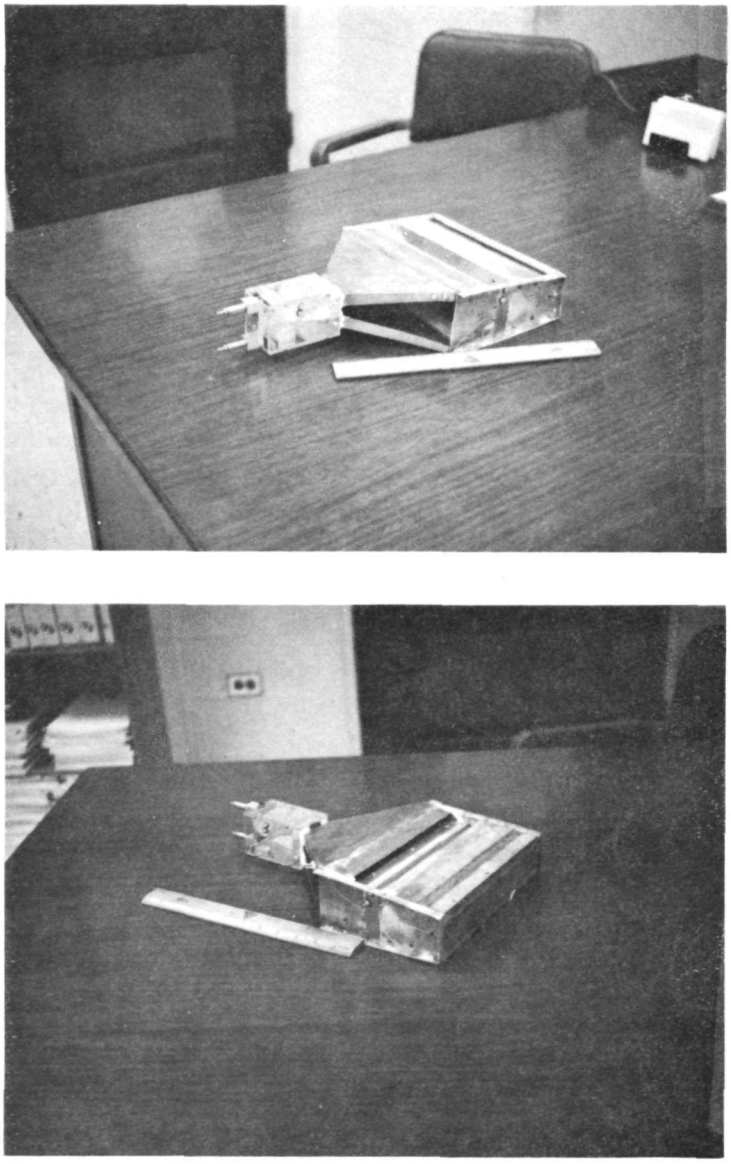

Figure 7. One Complete Assembly of Cascaded Fluidic Amplifiers

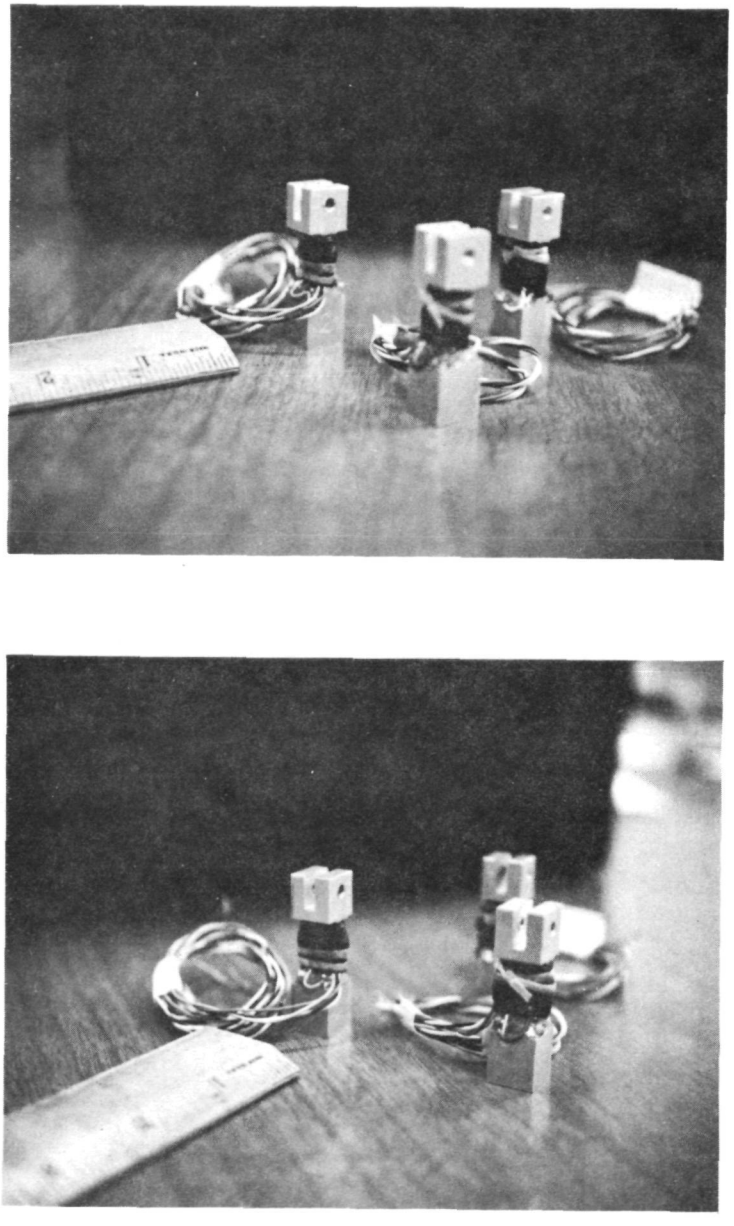

Figure 8. Model Mounting Attachments Fitted With Strain Gages

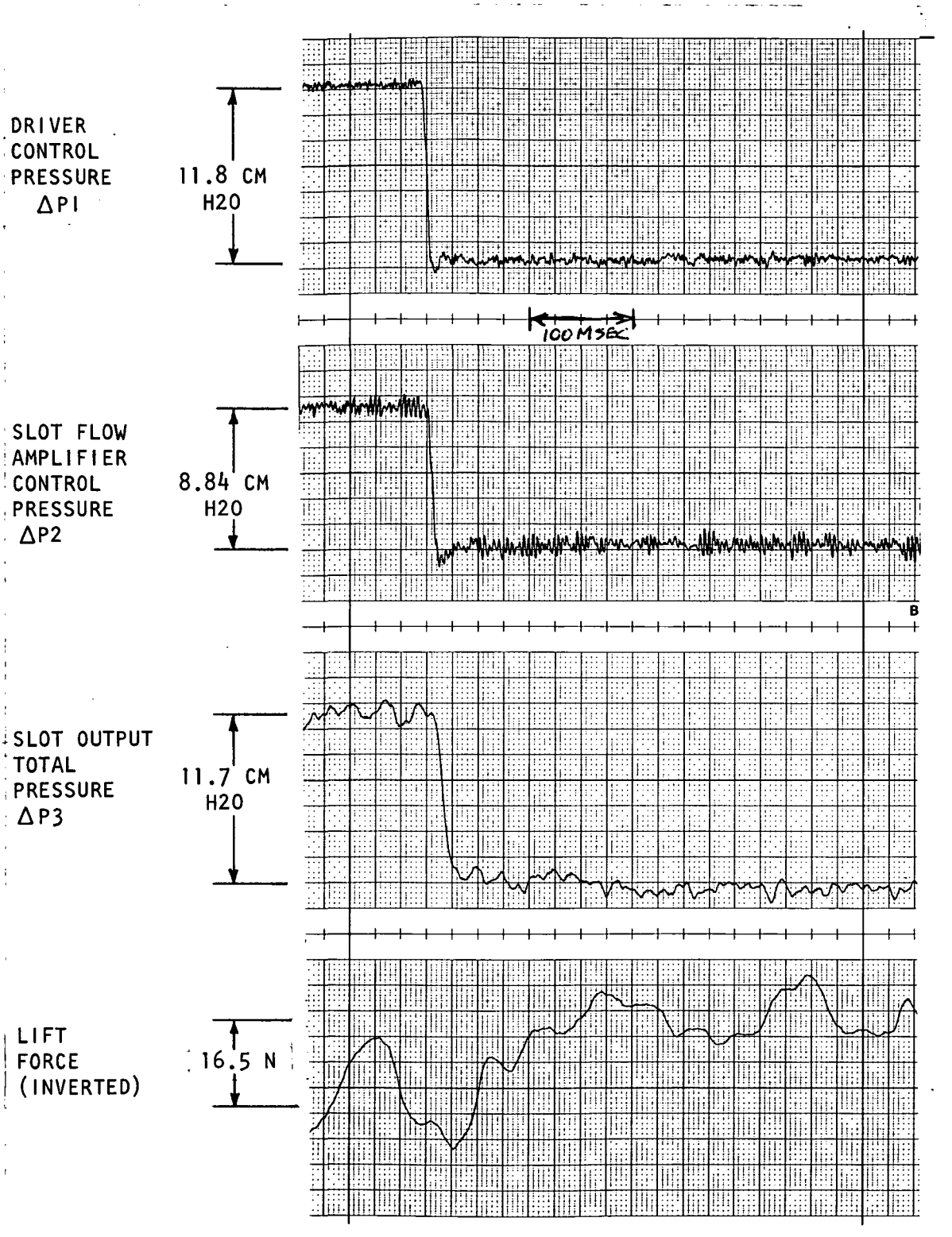

Figure 9. Typical Recording of Dynamic Test

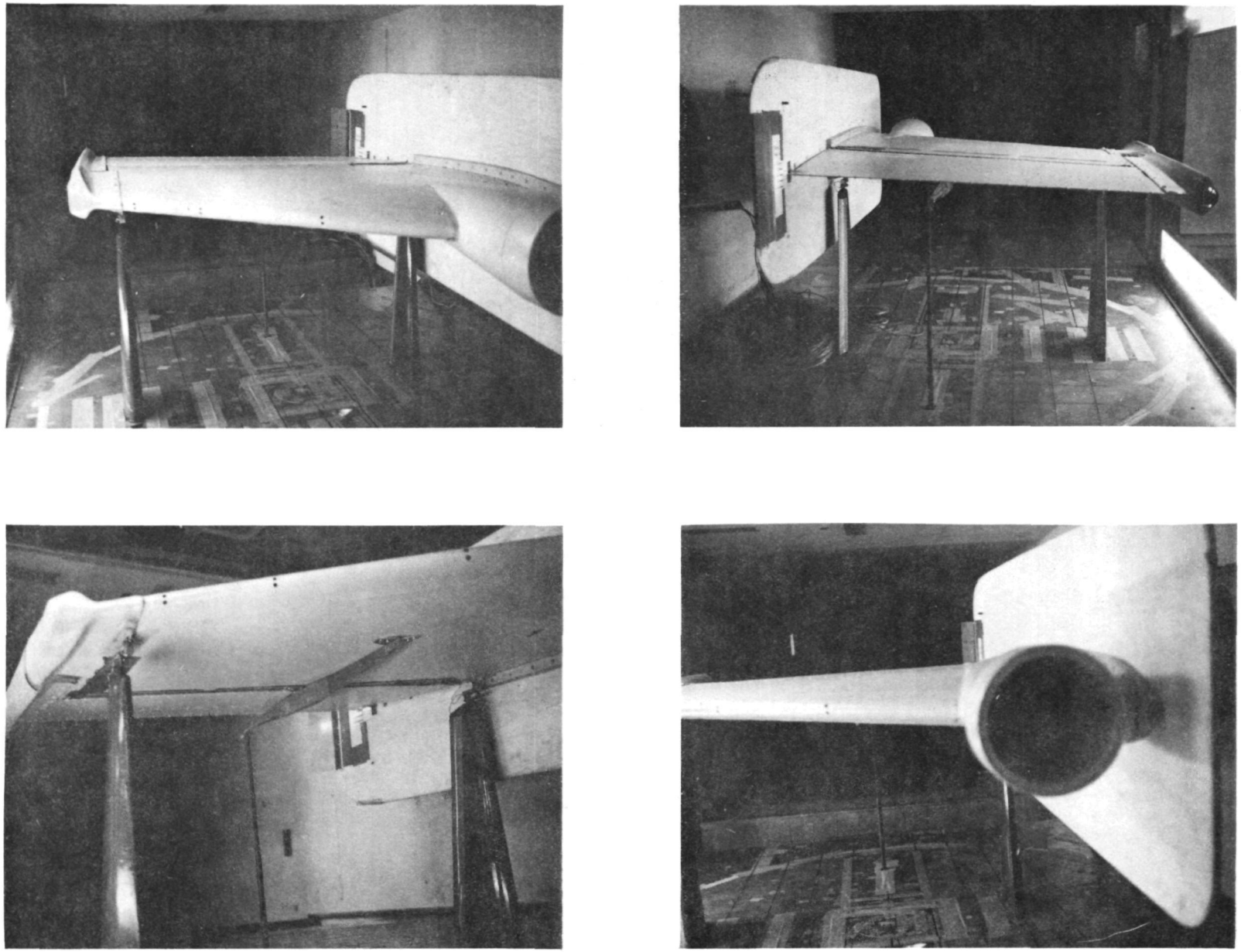

Figure 10. Phase 4 Fluidic Rudder in the Wind Tunnel

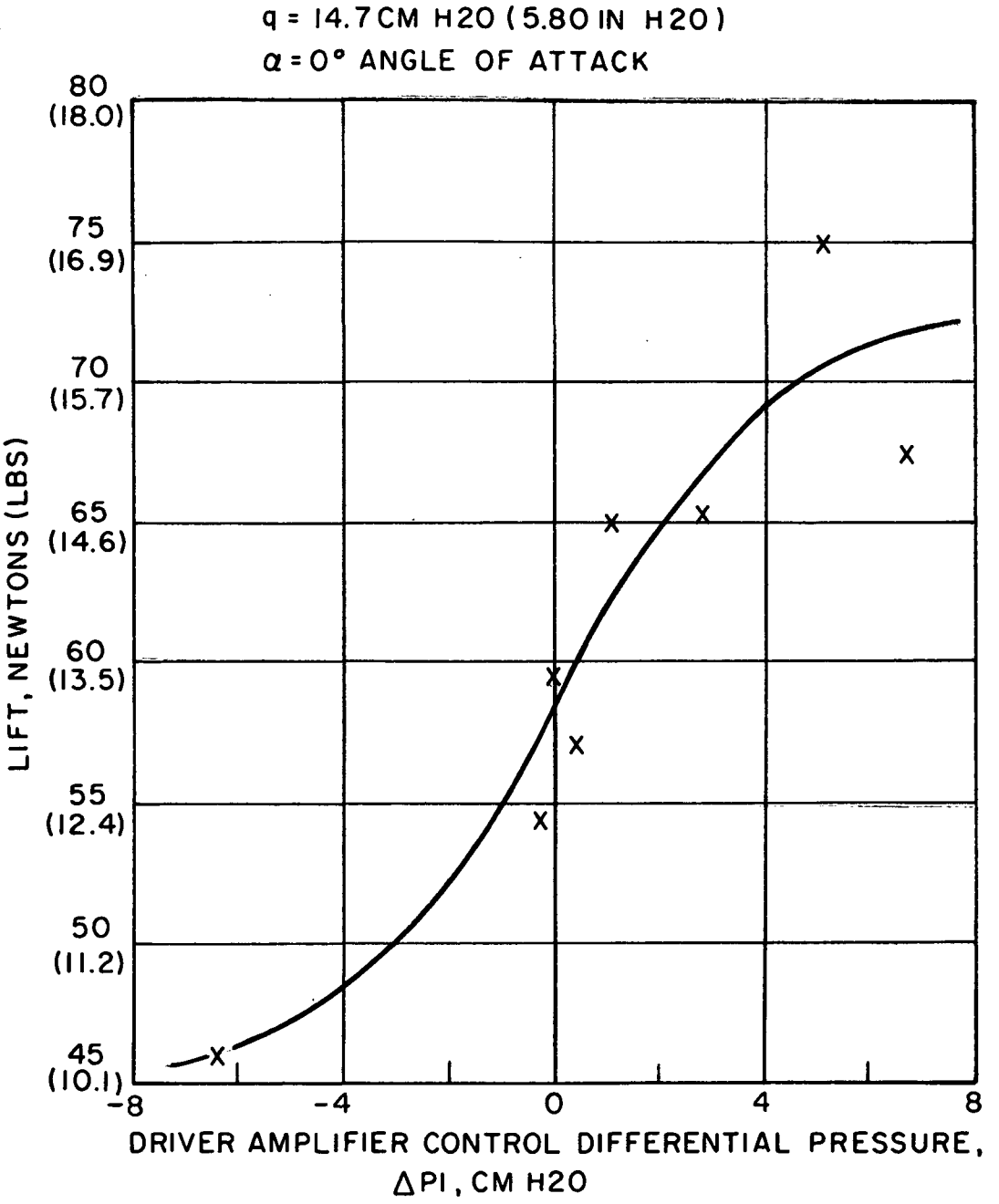

Figure 11. Lift Versus Driver Amplifier Signal

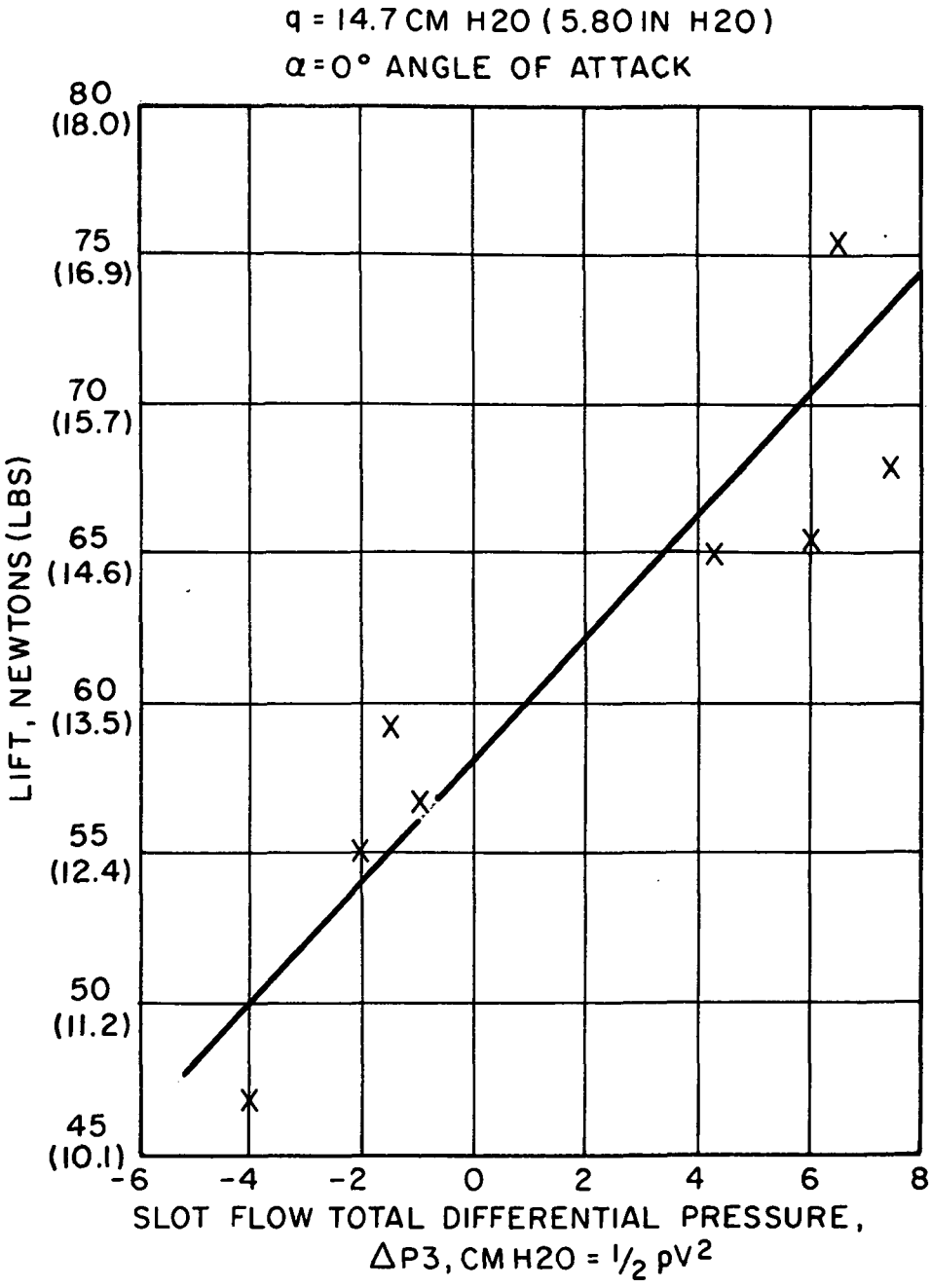

Figure 12. Lift Versus Airfoil Slot Flow

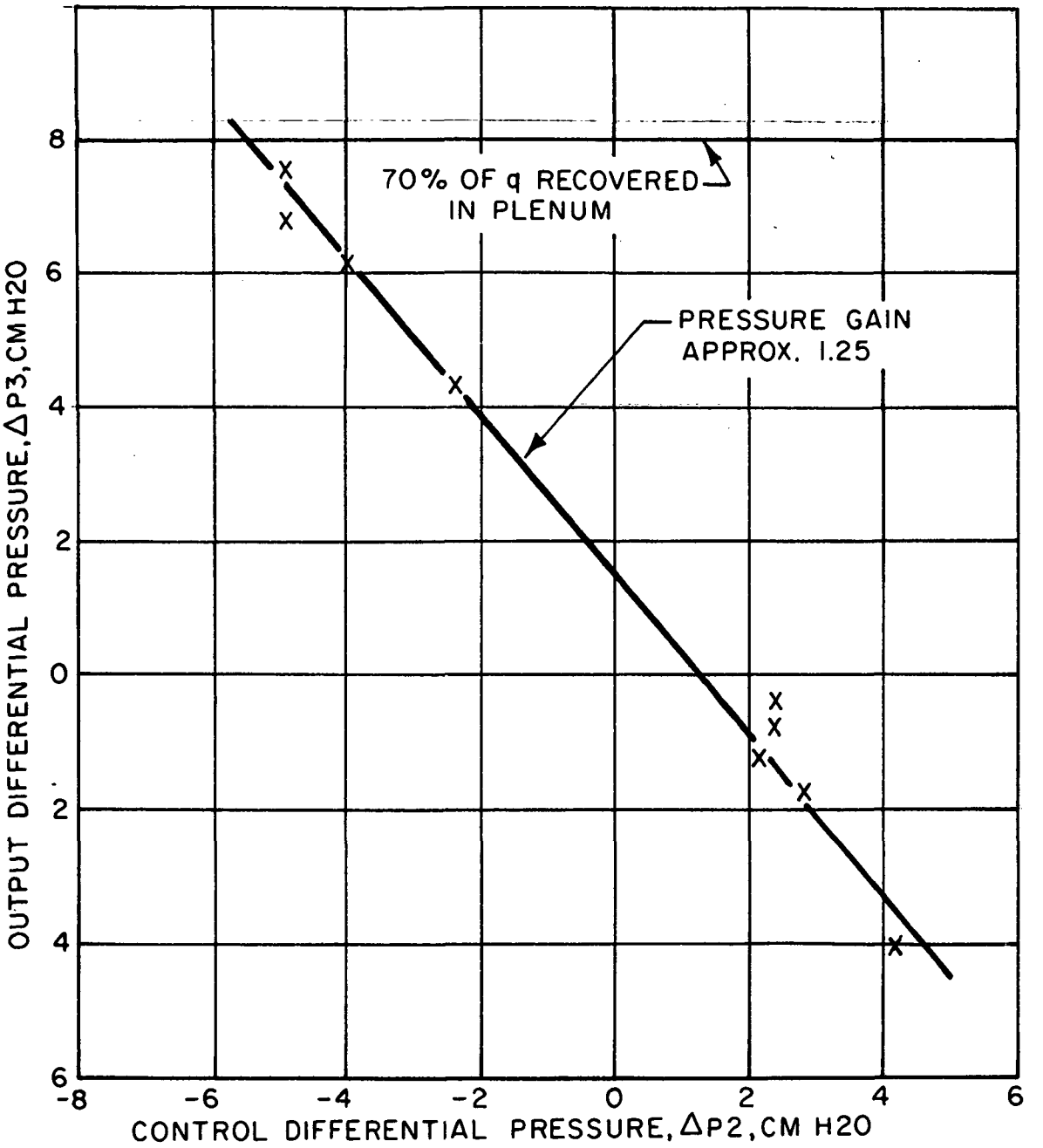

Figure 13. Static Characteristics of Slot Flow Amplifier

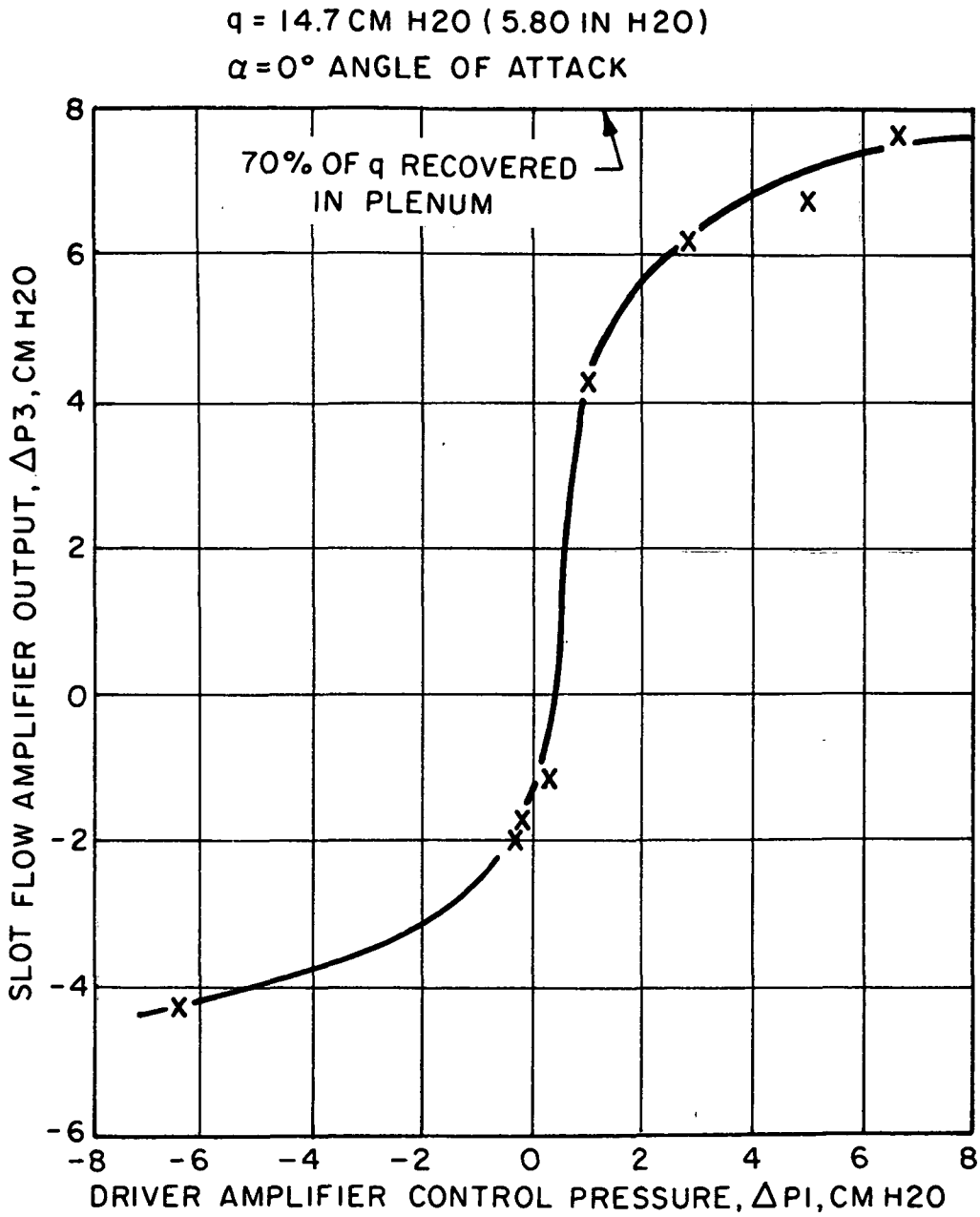

Figure 14. Static Characteristics of Cascaded Fluidic Amplifiers

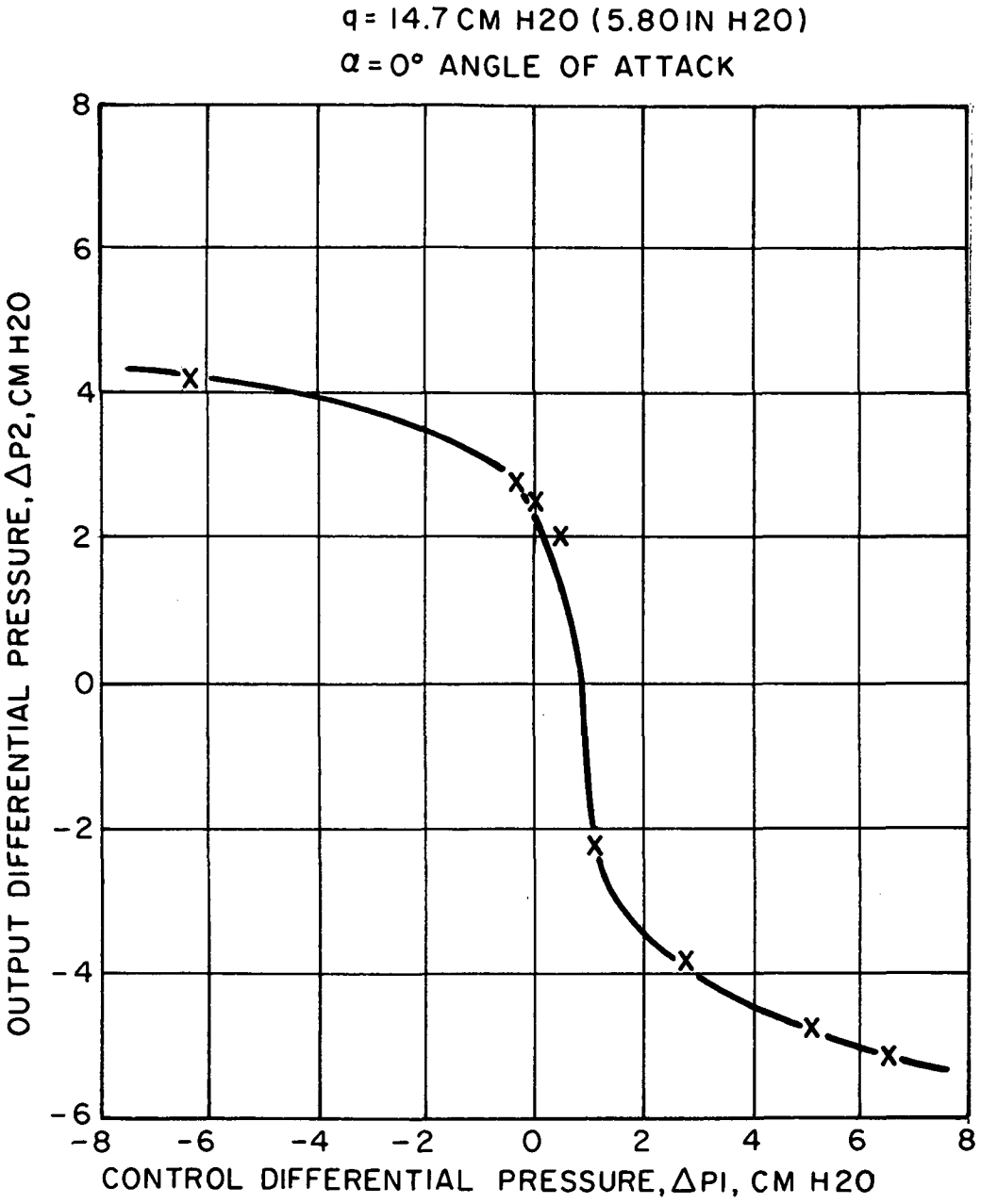

Figure 15. Static Characteristics of Driver Amplifier

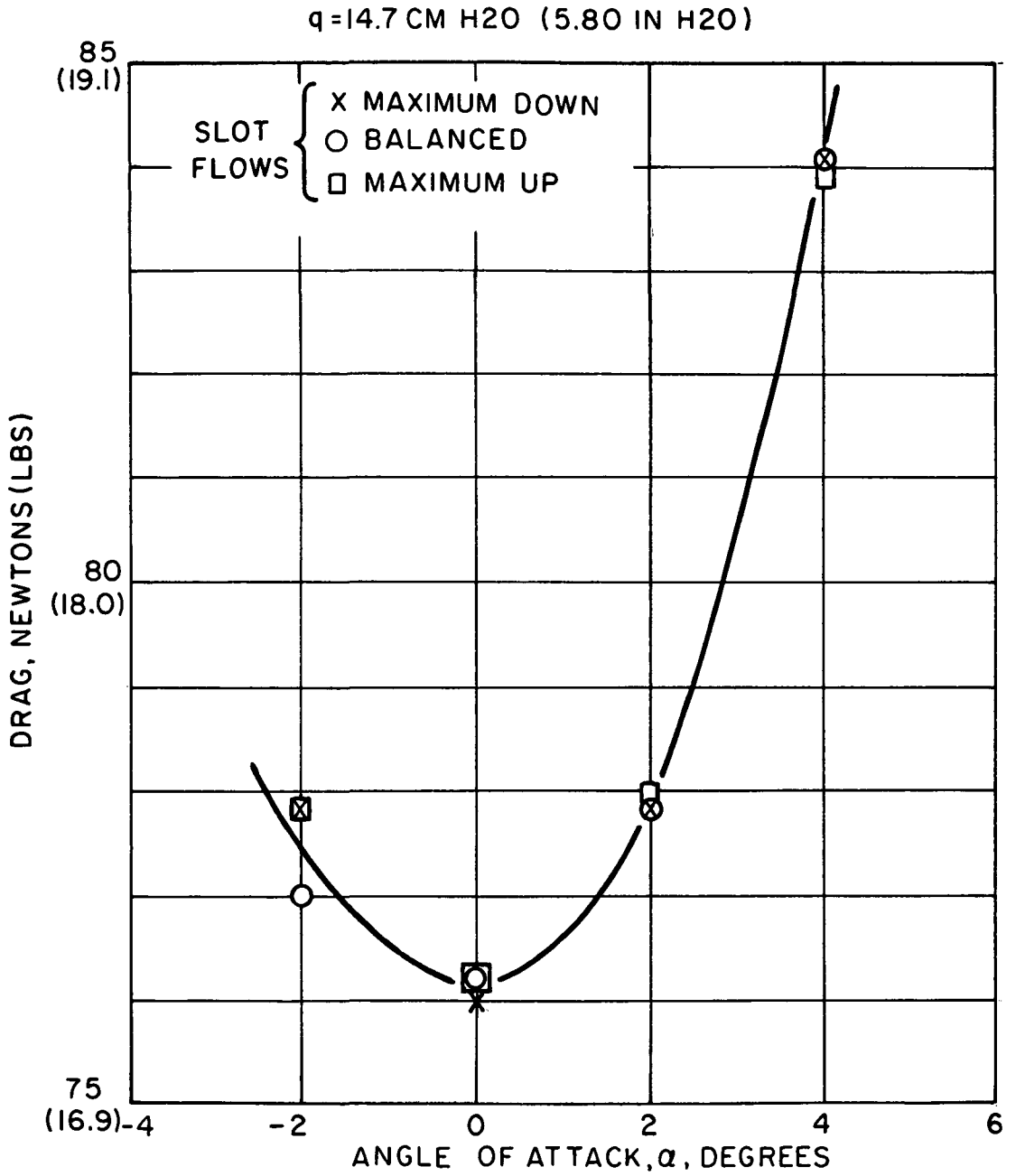

Figure 16. Drag Versus Angle of Attack (showing the effect of slot flow)

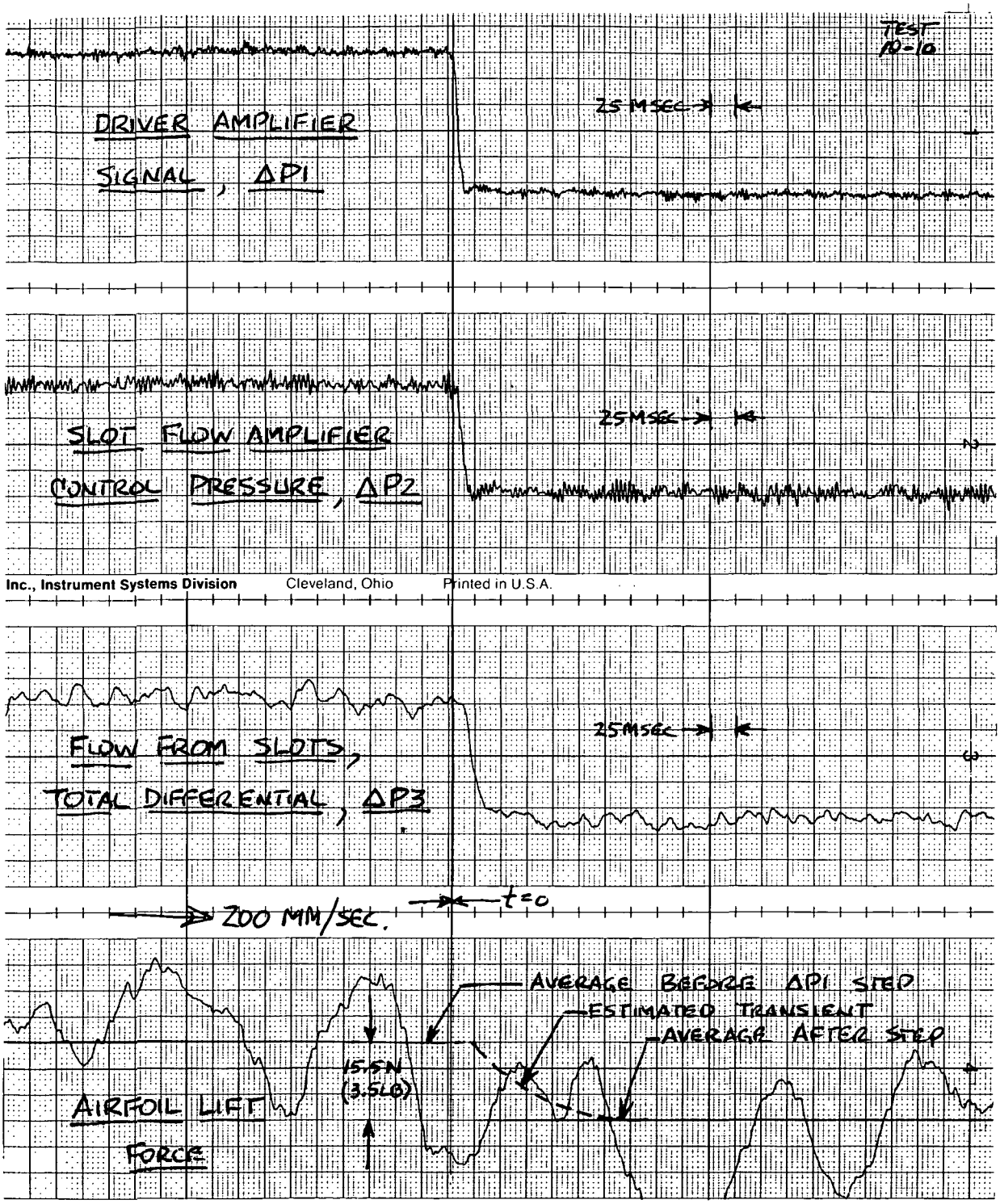

Figure 17. Dynamic Response of Fluidic Rudder - Lift

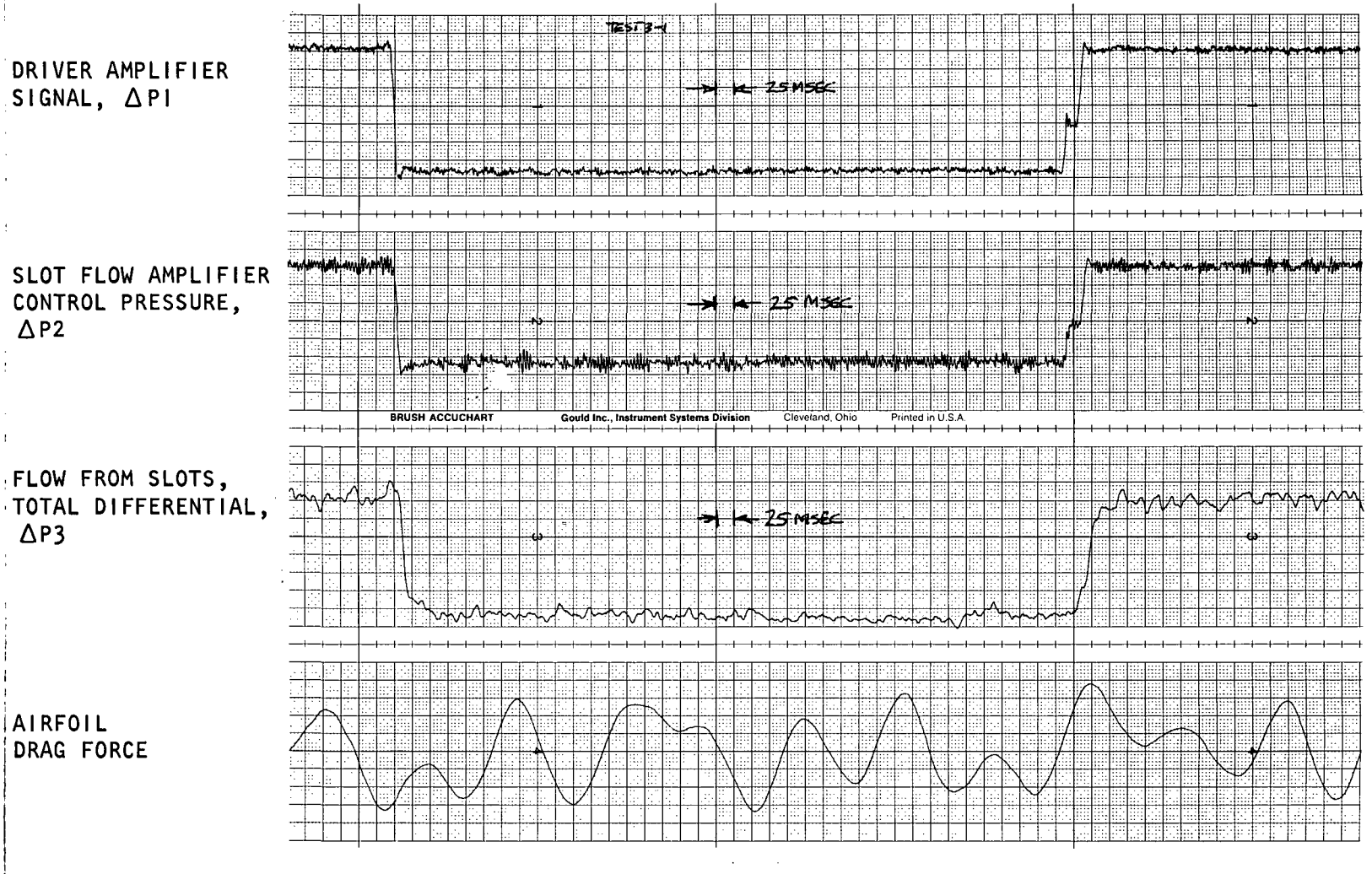

Figure 18. Dynamic Response of the Fluidic Rudder - Drag

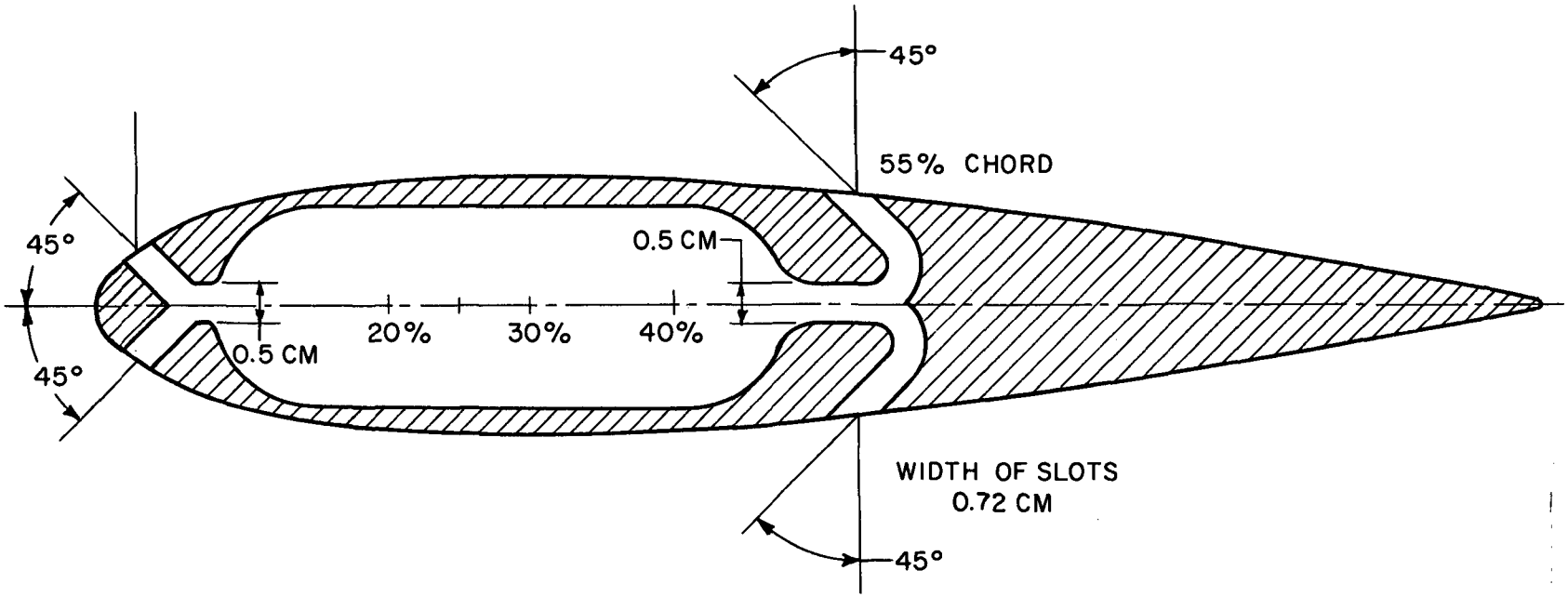

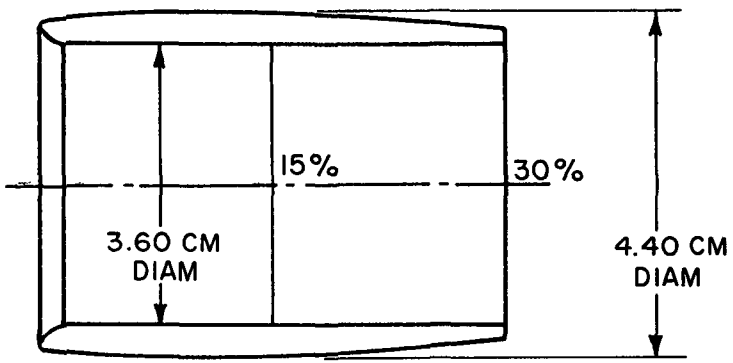

AIR SCOOP

CHORD 20.3 CM (8.0 IN.)
SPAN 19.0 CM (7.5 IN.)
AIR FOIL NACA 0018

Figure 19. Cross Section of Model 45 FWD

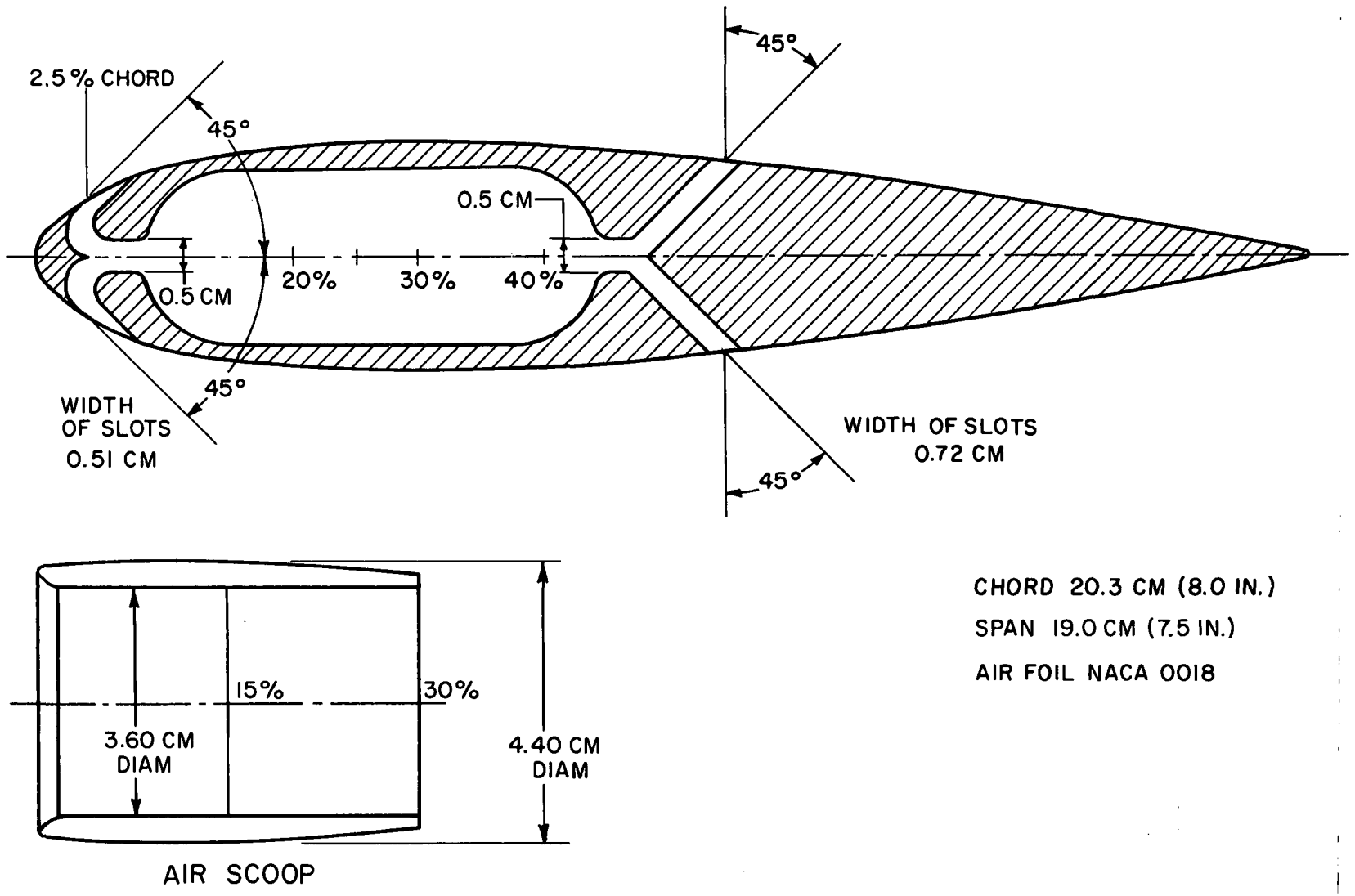

Figure 20. Cross Section of Model 45 AFT

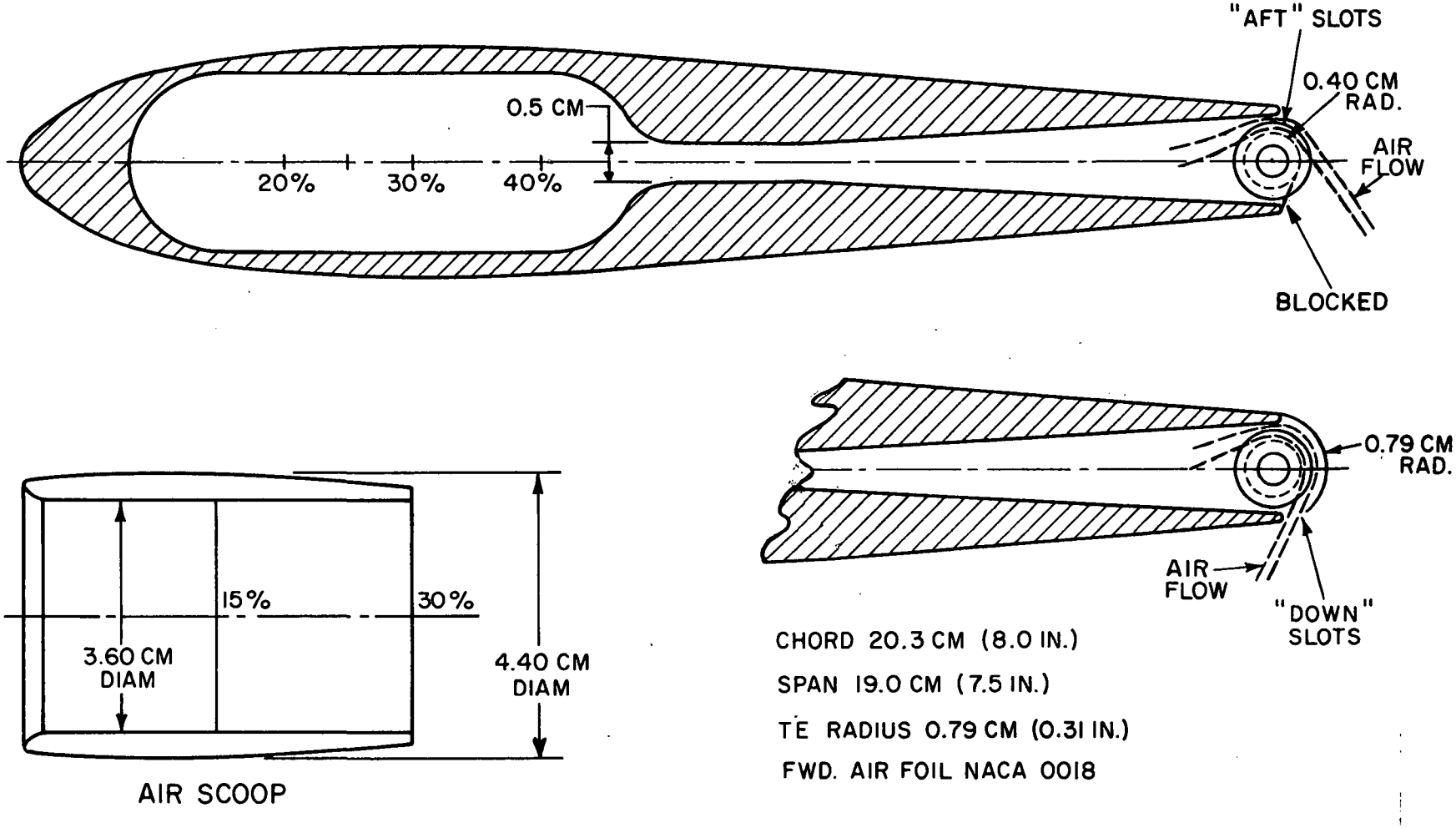

Figure 21. Cross Section of Model RTE

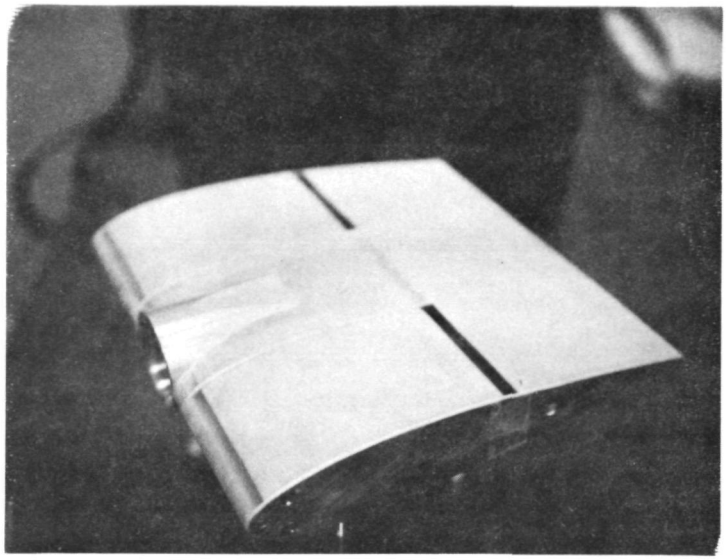

45 FWD

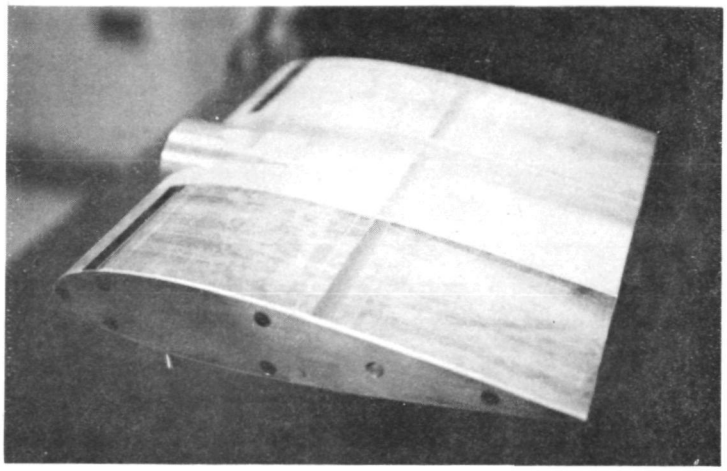

45 AFT

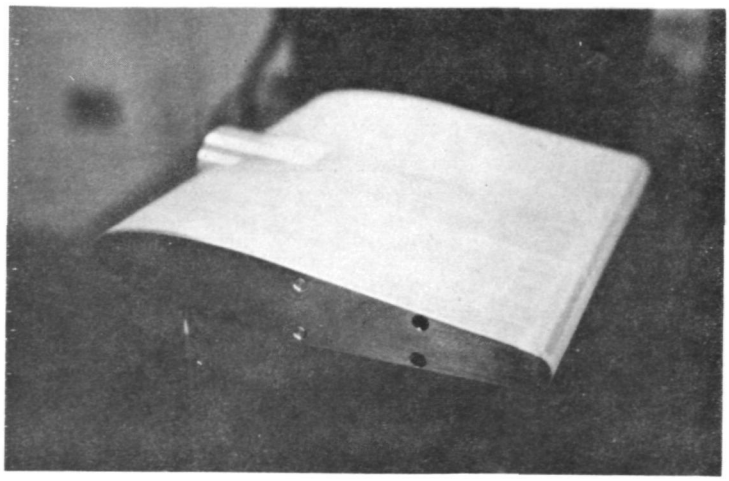

RTE

Figure 22. Photos of Three Airfoil Models, As Tested

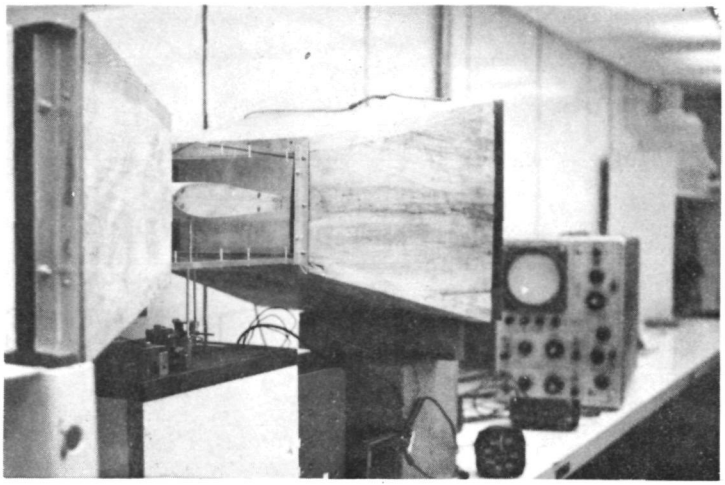

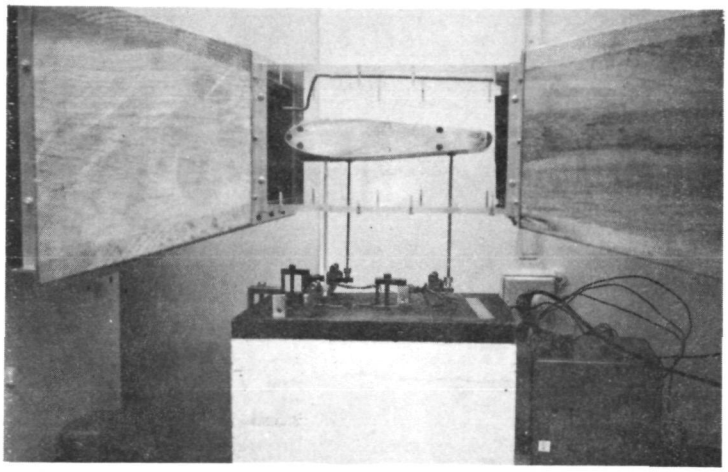

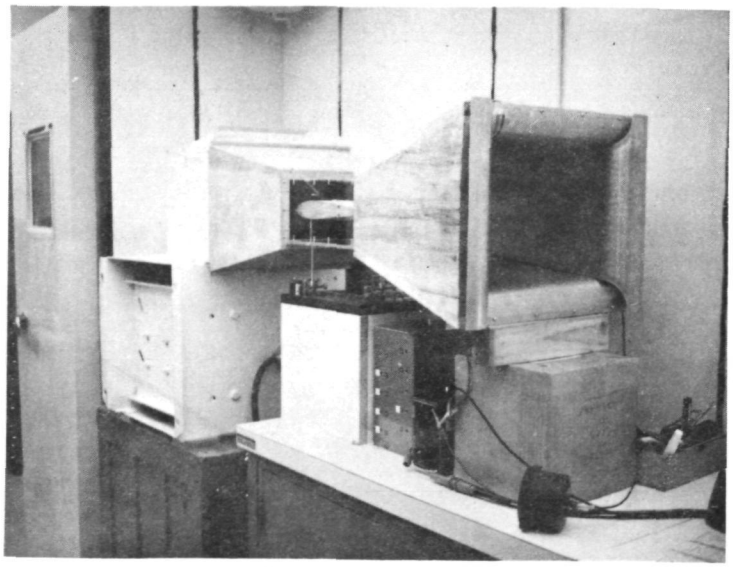

Figure 23. Model Test Facility

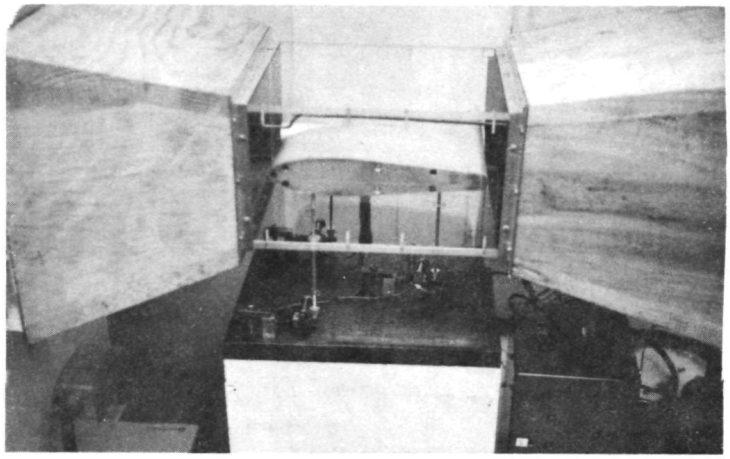

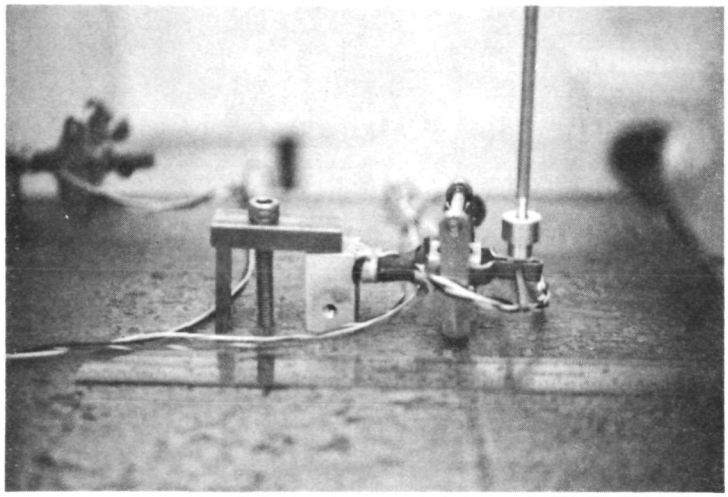

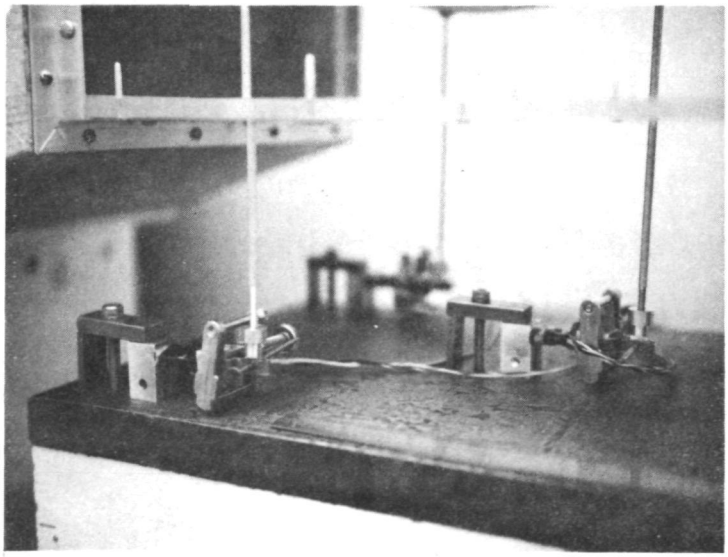

Figure 24. Strain-Gaged Attachments for Mounting Models

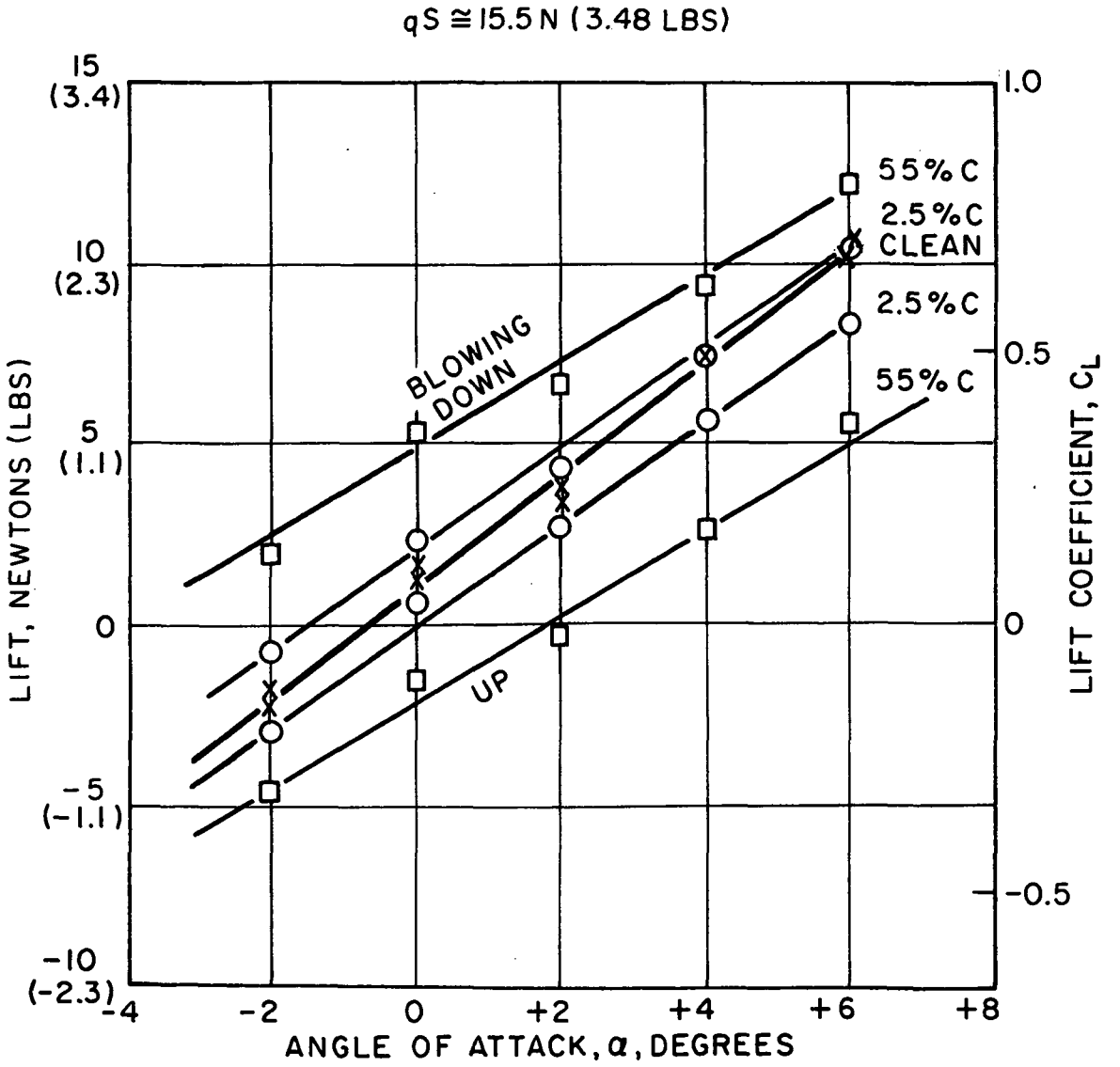

Figure 25. Characteristics of Model 45 FWD

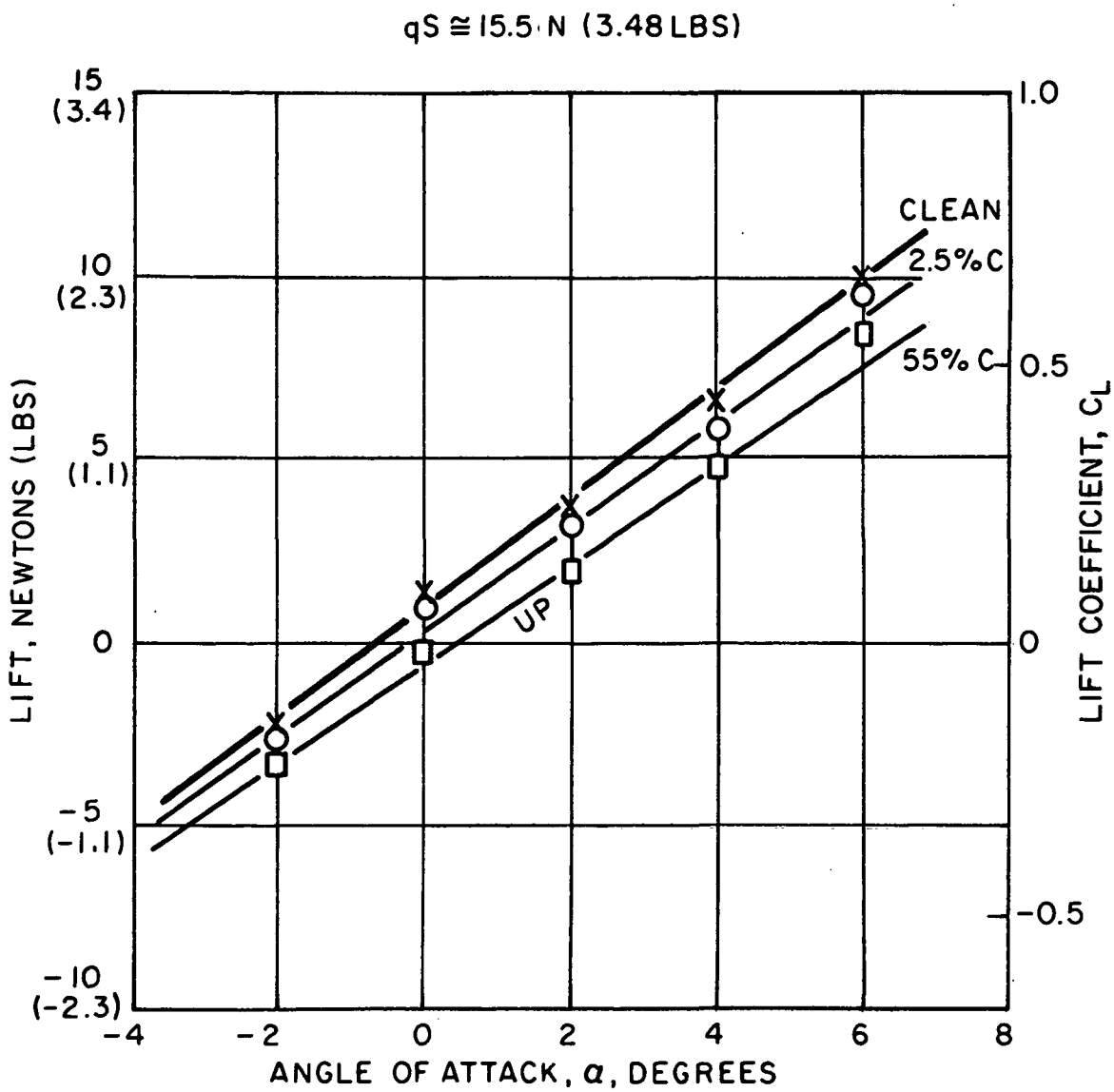

Figure 26. Characteristics of Model 45 AFT

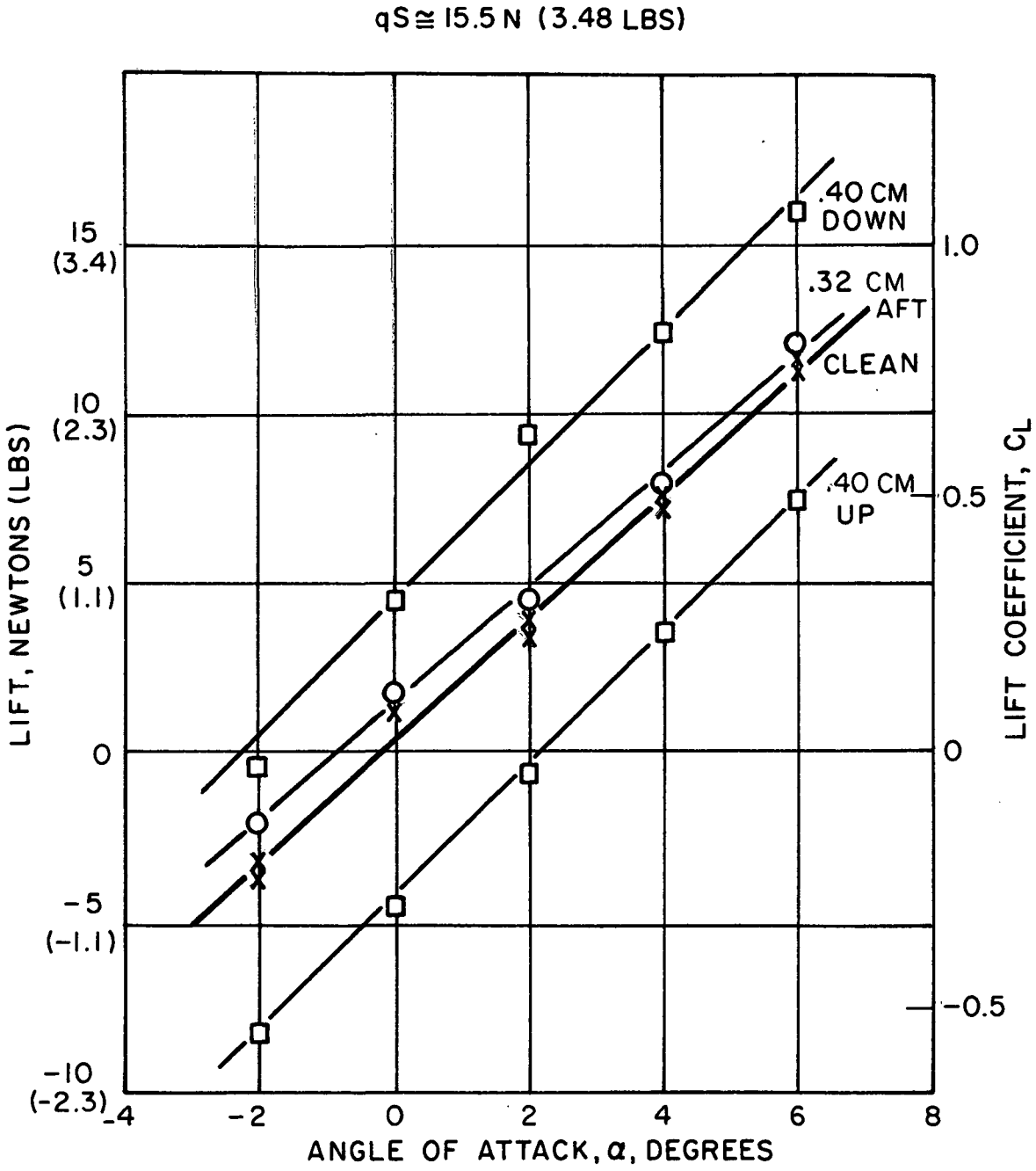

Figure 27. Characteristics of Model RTE

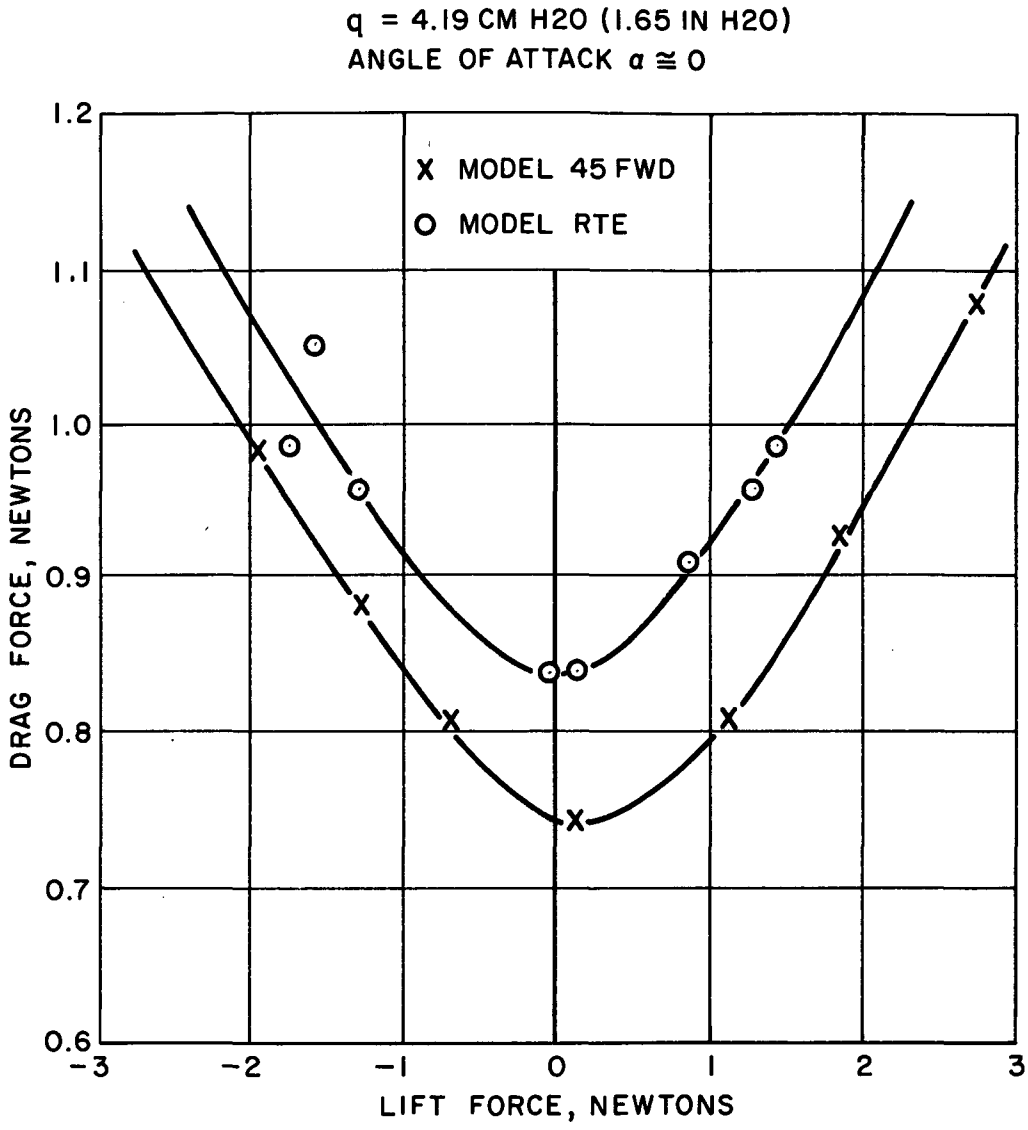

Figure 28. Drag Versus Lift for Models 45 FWD and RTE